iScience

CellPress
OPEN ACCESS

Article

Phosphatidylserine synthase plays an essential role in glia and affects development, as well as the maintenance of neuronal function

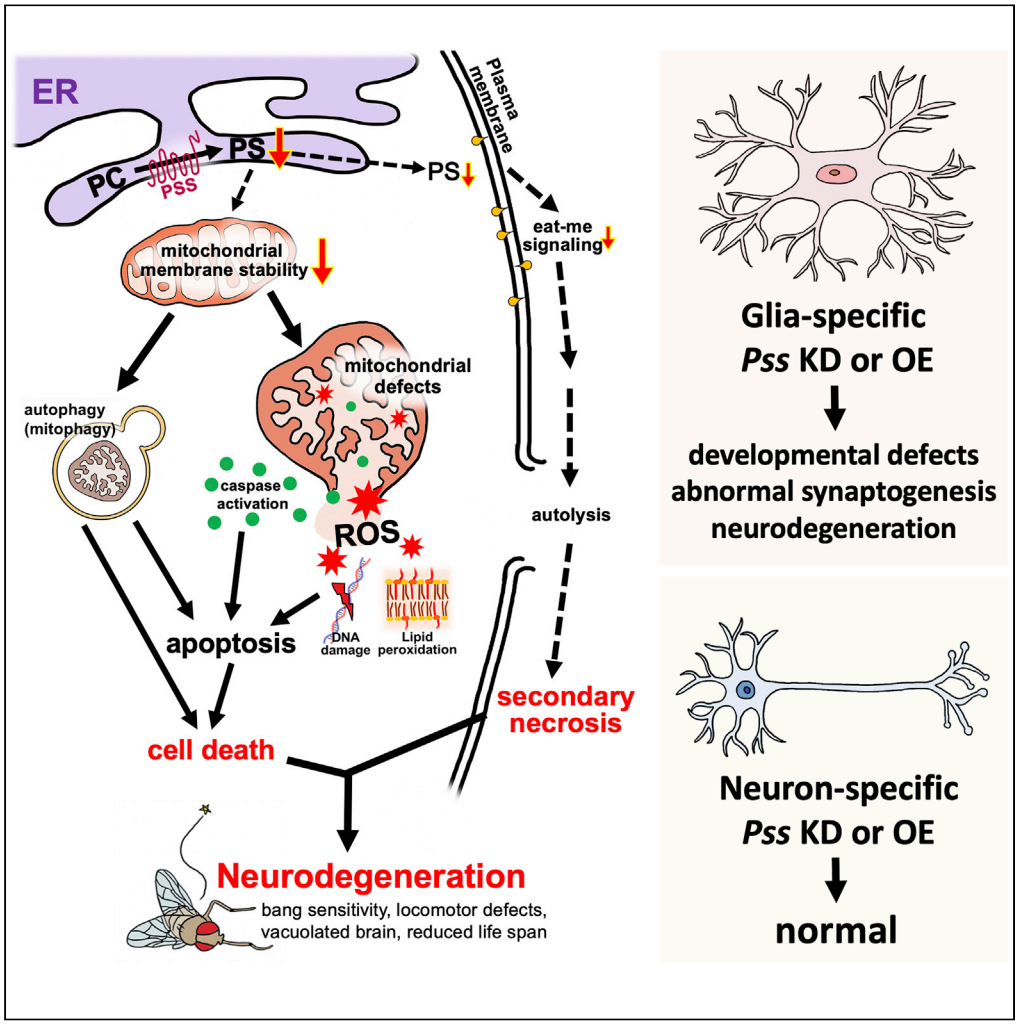

Ye-Jin Park, Sungkyung Kim, Hyeon-Pyo Shim, ..., Hugo J. Bellen, Seung-Hae Kwon, Sang-Hak Jeon

jeonsh@snu.ac.kr

Highlights

Loss of *Pss* leads to developmental defects and neurodegeneration

Loss of *Pss* causes a mitochondrial defect, elevated ROS, and secondary necrosis

Pss functions in glia are essential for synaptogenesis and neuronal maintenance

Glial *Pss* expression level must be tightly regulated to maintain a healthy nervous system

Park et al., iScience *24*, 102899
August 20, 2021
https://doi.org/10.1016/j.isci.2021.102899

iScience

CellPress
OPEN ACCESS

Article

Phosphatidylserine synthase plays an essential role in glia and affects development, as well as the maintenance of neuronal function

Ye-Jin Park,[1,5] Sungkyung Kim,[1] Hyeon-Pyo Shim,[2] Jae H. Park,[3] Gyunghee Lee,[3] Tae-Yeop Kim,[1] Min-Cue Jo,[1] Ah-Young Kwon,[1] Mihwa Lee,[1] Seongjae Lee,[1] Jiwon Yeo,[1] Hyung-Lok Chung,[5,6,7] Hugo J. Bellen,[5,6,7] Seung-Hae Kwon,[4] and Sang-Hak Jeon[1,8,*]

SUMMARY

Phosphatidylserine (PS) is an integral component of eukaryotic cell membranes and organelles. The *Drosophila* genome contains a single PS synthase (PSS)-encoding gene (*Pss*) homologous to mammalian PSSs. Flies with *Pss* loss-of-function alleles show a reduced life span, increased bang sensitivity, locomotor defects, and vacuolated brain, which are the signs associated with neurodegeneration. We observed defective mitochondria in mutant adult brain, as well as elevated production of reactive oxygen species, and an increase in autophagy and apoptotic cell death. Intriguingly, glial-specific knockdown or overexpression of *Pss* alters synaptogenesis and axonal growth in the larval stage, causes developmental arrest in pupal stages, and neurodegeneration in adults. This is not observed with pan-neuronal up- or down-regulation. These findings suggest that precisely regulated expression of *Pss* in glia is essential for the development and maintenance of brain function. We propose a mechanism that underlies these neurodegenerative phenotypes triggered by defective PS metabolism.

INTRODUCTION

Neurodegenerative diseases (NDs), like Alzheimer's disease (AD), Parkinson's disease (PD), Huntington's disease, and frontotemporal dementia, are a major threat to healthy aging as life expectancy has increased (Heemels, 2016). The best-characterized cause of ND is associated with protein aggregates, such as amyloid-β plaques and Tau-tangles in AD and α-synuclein in PD (Irvine et al., 2008; Ross and Poirier, 2004; Serpell and Smith, 2000; Sharon et al., 2003). Interestingly, some studies have shown changes in the phospholipid composition of neural tissue, including in patients with AD and PD (Buccoliero et al., 2004; Li et al., 2015; Pettegrew et al., 2001; Wang et al., 2014). Defective phospholipid biosynthetic enzymes are a likely cause of changes in phospholipid composition in ND models (Kretzschmar et al., 1997; Pavlidis et al., 1994). These studies speak to the important role of phospholipids in neural function. However, it is unclear whether changes in phospholipid composition are a consequence or a cause of ND.

Phosphatidylserine (PS) is one of the major phospholipids in cellular membrane and performs a variety of functions, including the regulation of intracellular signaling proteins such as protein kinase C (PKC), Akt, and Raf-1 (Kim et al., 2014). It also plays a role in the fusion of exocytotic vesicles with the plasma membrane (Williams et al., 2009) and acts as an "eat-me" signal for phagocytic clearance of apoptotic cells (Fadok et al., 1992; Leventis and Grinstein, 2010; Segawa and Nagata, 2015). Some clinical studies have shown that PS consumption significantly improves cognitive function and memory in patients with AD (Crook et al., 1991, 1992; Heiss et al., 1994). Furthermore, dietary intake of PS suppresses circadian and sleep disorders in PD models (Valadas et al., 2018). These results suggest a potentially important role for PS in the maintenance and/or function of neural tissues.

In mammals, PS is synthesized from phosphatidylcholine (PC) and phosphatidylethanolamine (PE) through enzymatic replacement of the head group with serine by two PS synthases, PSS1 for PC and PSS2 for PE (Vance and Steenbergen, 2005). Both enzymes are present in the endoplasmic reticulum (ER) and the mitochondria-associated membrane (MAM) (Stone and Vance, 2000). PS synthesized by PSS1 is transferred to

[1]Department of Science Education/Biology Education, Seoul National University, Seoul 08826, Republic of Korea

[2]Korea Institute for Curriculum and Evaluation, Chungcheongbuk-do 27873, Republic of Korea

[3]Department of Biochemistry & Cellular and Molecular Biology, and Neuronet Research Center, University of Tennessee, Knoxville 37996, USA

[4]Korea Basic Science Institute, Seoul Center 02841, Republic of Korea

[5]Department of Molecular and Human Genetics, Baylor College of Medicine, Houston, TX 77030, USA

[6]Jan and Dan Duncan Neurological Research Institute, Texas Children's Hospital, Houston, TX 77030, USA

[7]Howard Hughes Medical Institute, Baylor College of Medicine, Houston, TX 77030, USA

[8]Lead contact

*Correspondence: jeonsh@snu.ac.kr

https://doi.org/10.1016/j.isci.2021.102899

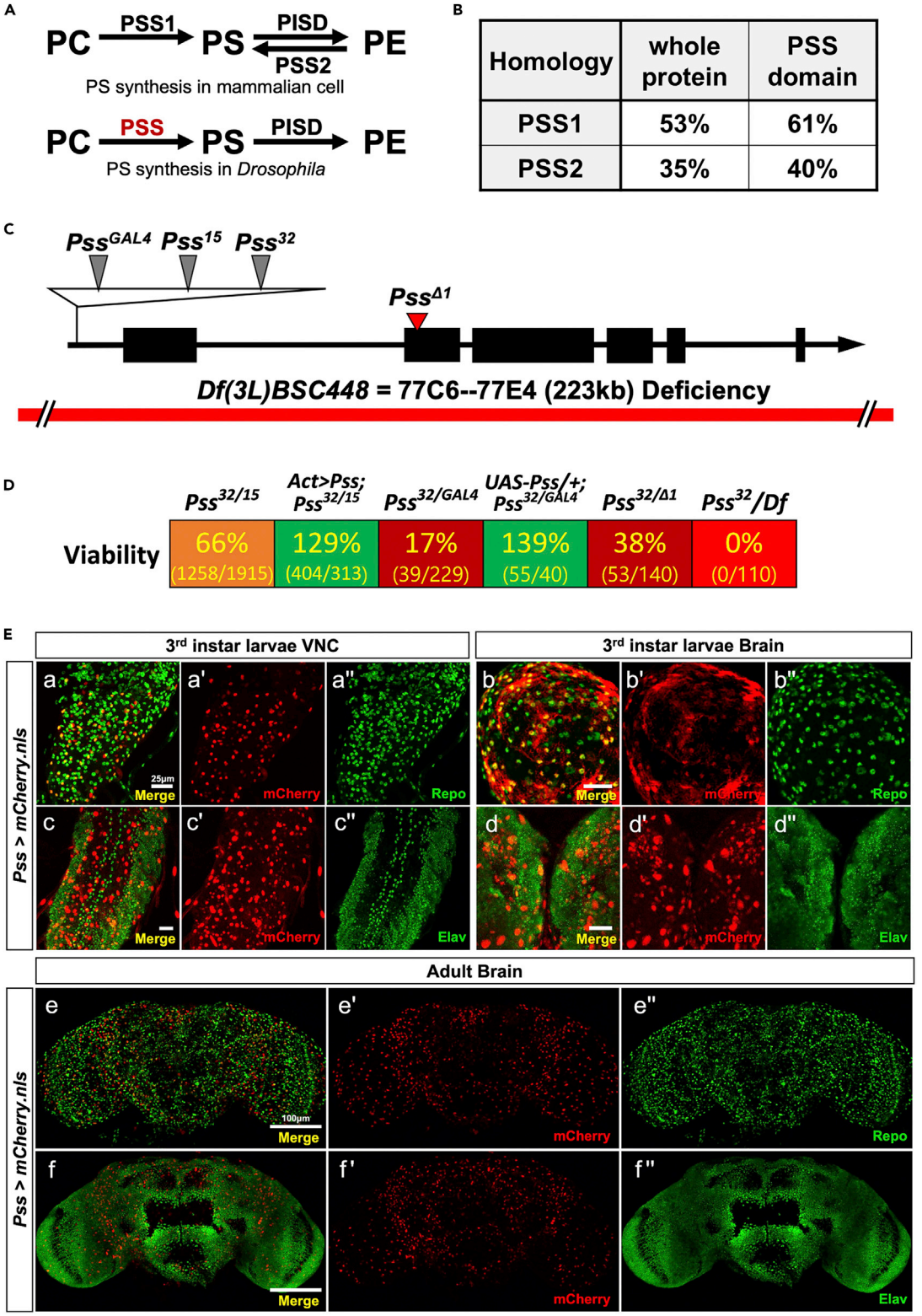

Figure 1. The fly *Pss* gene: structure and expression pattern

(A) PS synthesis in mammalian cell and *Drosophila*. *Drosophila* PSS is the only PS synthase in *Drosophila*.

(B) Homology between *Drosophila* PSS and human PSS1 and PSS2.

Figure 1. *Continued*

(C) *Pss* mutant alleles. Three *P* element insertions are clustered in a small region of the 5′ UTR. Pss^{41} is a deletion mutation in the second exon, which causes a frameshift in the ORF.

(D) Complementation tests. The *trans*-heterozygous mutants are in the same w^+ background as we used the Pss^{32} line to collect virgins for crosses. With the ubiquitous overexpression of *Pss*, the viabilities of *trans*-heterozygous mutants were increased up to 139% of expected flies. Numbers indicate the ratio of observed/expected flies.

(E) Identification of cell types expressing *Pss* in the larval CNS and adult brain. mCherry expression by *Pss-GAL4* (*Pss>mCherry.nls*) in the third instar larval (a′, c′) ventral nerve cord (VNC) and (b′, d′) brain, and (e′, f′) adult brain. (a", b", e") Glial cells were labeled by anti-Repo and (c", d", f") neuronal cells by anti-Elav. (a-f) Merged image of *Pss>mCherry.nls* with either anti-Repo or anti-Elav. Scale bar, 25 μm in a-d, 100 μm in e-f.

the mitochondria, where it is converted into PE by PS decarboxylase (Choi et al., 2005) (Figure 1A). PE and PS also migrate to the Golgi apparatus and then to the plasma membrane using vesicular transport mode (Leventis and Grinstein, 2010). Mice that carry a loss-of-function mutation for either PSS1 ($Pss1^{-/-}$) or PSS2 ($Pss2^{-/-}$) are viable, but double knockout mice ($Pss1^{-/-}$; $Pss2^{-/-}$) are prenatally lethal, indicating that PSS1 and PSS2 have a redundant function (Arikketh et al., 2008; Bergo et al., 2002). Mutations in human PSS1 (*PTDSS1*) cause Lenz-Majewski hyperostotic dwarfism (LMHD), a rare disease characterized by multiple congenital anomalies featuring generalized craniotubular hyperostosis, developmental defects, and intellectual disability (Sousa et al., 2014). However, the mechanisms underlying the association between *PTDSS1* function and the neural defects seen in LMHD are not known.

In this study, we report that loss of *Pss* causes neurodegenerative features, including reduced life span, increased bang sensitivity, locomotor defects, and increased formation of vacuoles in the brain observed. In addition, we document that glial-specific knockdown or overexpression of *Pss* caused altered synaptogenesis and axonal growth in the larval stage, developmental arrest in pupae, and neurodegeneration in the adults, indicating that PSS plays a critical role in glia.

RESULTS

Pss encodes a *Drosophila* homolog of mammalian *PSS* genes

The *Drosophila* genome contains a single PSS-encoding gene (*Pss*) (Figure 1A) (Midorikawa et al., 2010; Vance and Steenbergen, 2005; Vance and Tasseva, 2013). It is the homolog to both human PSS1 and PSS2 (Figure 1B). *Drosophila* PSS exhibits 53% homology to human PSS1 across the entire sequence, and PSS and PSS1 share a well-conserved PSS domain with 61% homology (DIOPT score 15 of 15) (Hu et al., 2011). *Drosophila* PSS shares 35% homology across the entire PSS2 protein and 40% homology in the PSS domain (DIOPT score 3 of 15), indicating that *Drosophila* PSS is more closely related to PSS1 than PSS2 (Figure S1A).

To delve into a function of *Pss in vivo*, we characterized three different *P* element insertion lines (Pss^{15}, Pss^{32}, Pss^{GAL4}) inserted in the 5′ UTR of the *Pss* gene (Figures 1C and S1B). We also generated a deletion mutation (Pss^{41}) by removing 14 bp in the second exon using the CRISPR/Cas9 strategy (Kondo and Ueda, 2013). This deletion causes a frameshift in the ORF of *Pss*, suggesting it is a null-allele. These alleles (Pss^{15}, Pss^{32}, Pss^{GAL4}, Pss^{41}) are all homozygous embryonic lethal, and Pss^{GAL4}/Pss^{GAL4} animals can be rescued to pharate adults with *UAS-Pss* (Figure S1C). Complementation tests show that some alleles partially complement each other and produce *trans*-heterozygous viable adults (Figure 1D). As the Pss^{15}, Pss^{GAL4}, and Pss^{41} are not in the w^+ background, we used the Pss^{32} ($P\{PZ\}Pss^{04521}$ $ry^{506}/TM3$, ry^{RK} Sb^1 Ser^1) as female parent to make the *trans*-heterozygous mutants with the same w^+ background. When we cross two different *Pss* heterozygous mutant flies to generate *trans*-heterozygous progenies, we also get heterozygous progenies of two different genotypes. We counted the number of all heterozygous progenies, and half of them would be the theoretically expected number of *trans*-heterozygotes. The reduced viability of these *trans*-heterozygous animals can be rescued by *actin-GAL4* or *Pss-GAL4>UAS-Pss* showing that they indeed affect *Pss* (Figure 1D) and result in partial loss of function of PSS (Figures 2A and S1D). To assess the level of *Pss* transcripts in *Pss* mutant flies, we used quantitative RT-PCR (qRT-PCR), which showed that *trans*-heterozygous flies have an 84–88% reduction in *Pss* expression compared with wild-type flies (*Canton-S*), while heterozygous flies showed an approximately 65% reduction when compared with wild-type flies (Figures 2A and S1D). We, therefore, performed the experiments using *trans*-heterozygous mutant flies to examine the function of *Pss* in larvae and adults. We selected the weakest allelic combination Pss^{32}/Pss^{15} for most experiments.

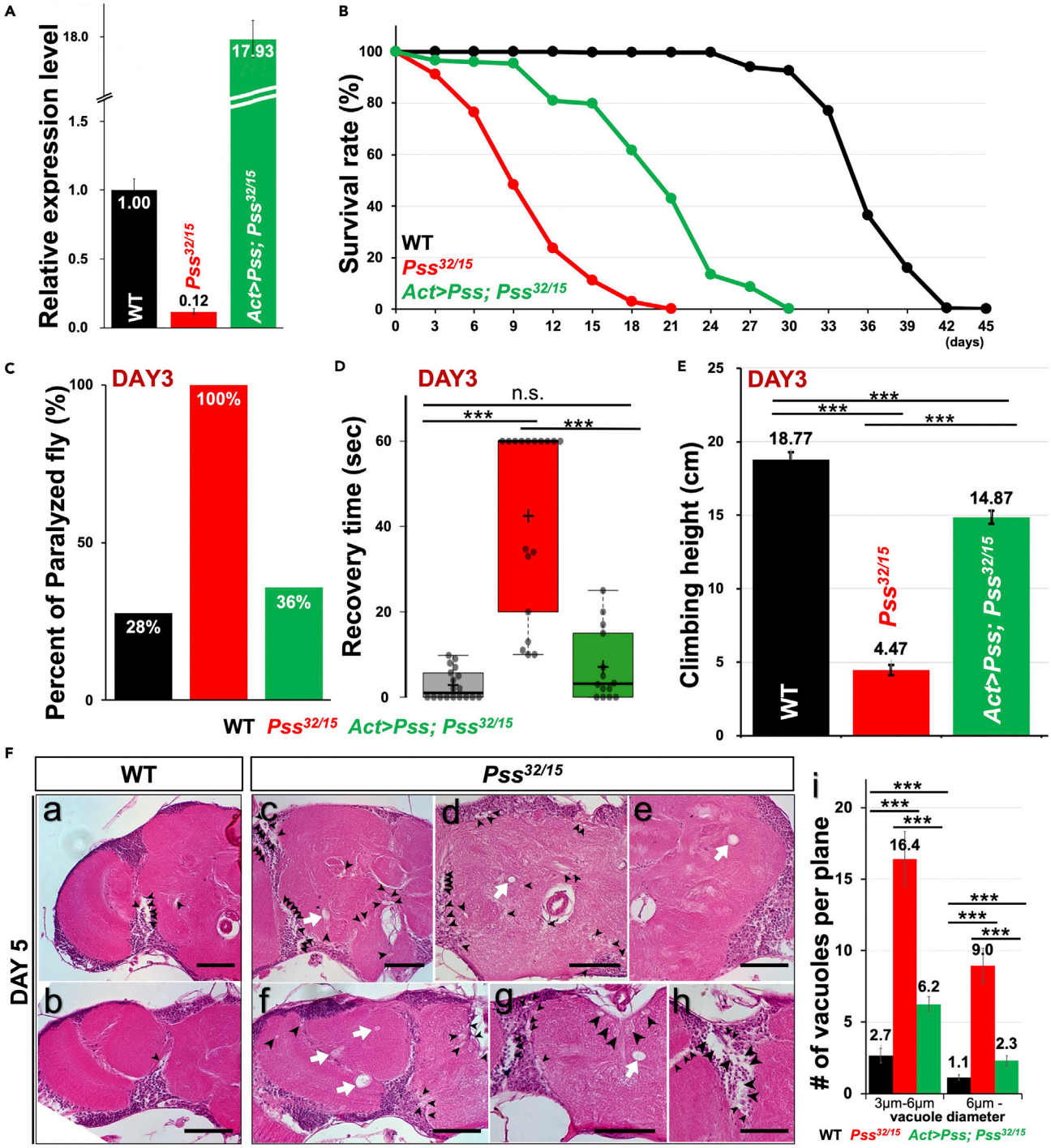

Figure 2. *Pss* mutants exhibit neurodegenerative phenotypes

(A) qRT-PCR showing *Pss* expression levels in $Pss^{32/15}$ flies and *Act>Pss;* $Pss^{32/15}$ flies compared with the wild type (WT). Bars represent max and min values.

(B) Survival curves at 29°C. WT n = 200, $Pss^{32/15}$ n = 199, *Act>Pss;* $Pss^{32/15}$ n = 172 (Log rank test: $p < 0.0001$).

(C and D) Bang-sensitive phenotypes of 3-day-old flies. (C) *Trans*-heterozygous *Pss* mutants were more sensitive to shock than wild-type flies and rescue flies.

(D) Recovery time for paralyzed flies. *Pss* mutant flies took longer to recover (WT 2.9 sec, $Pss^{32/15}$ 42.5 sec, *Act>Pss;* $Pss^{32/15}$ 7.1 sec). Bars represent mean ± SEM. ***$p < 0.001$; n.s., not significant. Numbers within the bars indicate mean values. WT n = 18, $Pss^{32/15}$ n = 18, *Act>Pss;* $Pss^{32/15}$ n = 14.

(E) *Pss* mutation reduces the flies' climbing ability. Climbing assays were analyzed in 3-day-old flies of the indicated genotypes. Bars represent mean ± SEM. ***$p < 0.001$. The numbers above the bars indicate mean values. WT n = 100, $Pss^{32/15}$ n = 100, *Act>Pss;* $Pss^{32/15}$ n = 100.

Figure 2. *Continued*

(F) Head sections showing vacuoles in the brains of 5-day-old flies. Vacuoles were significantly more abundant in $Pss^{32/15}$ mutant brains. Some of the vacuoles are indicated by black arrowheads or white arrows. **(a, b)** WT. **(c-h)** *Trans*-heterozygous *Pss* mutants. Scale bar, 50 μm. **(i)** quantification of vacuoles. $Pss^{32/15}$ flies with *Actin-GAL4* and *UAS-Pss* partially rescued the vacuolization. Bars represent mean ± SEM. ***p < 0.001. Numbers above the bars indicate mean values. WT n = 13, $Pss^{32/15}$ n = 11, *Act>Pss;* $Pss^{32/15}$ n = 14.

The loss of one copy of *Pss* does not exhibit any obvious behavior or morphological defects right after eclosion, but *trans*-heterozygous escapers ($Pss^{32/15}$, $Pss^{32/GAL4}$, $Pss^{32/\Delta 1}$) exhibit severe movement defects and are barely mobile. To assess if PSS is expressed in the central nervous system (CNS), we crossed Pss^{GAL4} with *UAS-mCherry.nls or UAS-GFP.nls* to mark the nuclei of cells expressing *Pss* (Figure 1E). Interestingly, mCherry-expressing cells were co-labeled mostly with subsets of Repo-positive cells (Figure 1E a, b, e) and few Elav-positive cells (Figure 1E c, d, f), indicating that *Pss* is highly enriched in subsets of glia in the CNS. In addition, *Pss* is also expressed in some other tissues such as salivary gland (sg), fat body (fb), gut (g), trachea (tc), and oenocytes (oc) besides the nervous system (Figure S1E).

Pss mutants exhibit neurodegenerative phenotypes

The life span of $Pss^{32/15}$ flies is significantly reduced, and most flies die within 12 days (Figure 2B). The mean T50 (time at 50% survival) of $Pss^{32/15}$ flies was 9.6 days, whereas the T50 for wild-type flies was 36 days. The $Pss^{32/15}$ flies that contain *Actin-GAL4>UAS-Pss* showed a partially rescued life span with a T50 of 22.8 days. The $Pss^{32/+}$ and $Pss^{\Delta 1/+}$ flies showed no reduction in life span compared with wild-type flies (Figure S1F).

We also examined $Pss^{32/15}$ flies for bang sensitivity and climbing ability. Bang sensitivity assay can induce seizures in flies (Kuebler and Tanouye, 2000; Parker et al., 2011). Upon vortexing the flies for 5 sec, wild-type flies right themselves within a few seconds, but flies that are sensitive show stereotypical cycles of shaking and paralysis for many seconds and up to minutes. We used 3-day-old adults. $Pss^{32/15}$ flies showed significant shock-induced paralysis (100%) when compared with wild-type flies (28%). Ubiquitous expression of *Pss* (*Act>UAS-Pss*) rescues (36%) the Bang sensitivity of $Pss^{32/15}$ flies (Figure 2C). We also measured recovery time from shock-induced paralysis, and $Pss^{32/15}$ flies took significantly longer to recover when compared with wild-type flies and rescue flies (2.9 sec on average for wild-type flies, 7.1 sec for rescue flies vs. 42.5 sec for $Pss^{32/15}$ mutants) (Figure 2D).

We also performed climbing test in 3-day-old wild-type flies climbed above 18 cm on average in 10 sec, whereas $Pss^{32/15}$ mutants managed only 4.47 cm (Figure 2E). Ubiquitous expression of *Pss* (*Act>UAS-Pss*) partially rescues the climbing defects of $Pss^{32/15}$ flies (Figure 2E). We further noticed that heterozygous *Pss* ($Pss^{32/+}$ and $Pss^{\Delta 1/+}$) flies exhibit a progressive decline in locomotion (Figure S1G). These results suggest that *Pss* heterozygosity does not affect longevity but does affect certain behaviors with age, such as climbing ability. In summary, a severe loss of *Pss* causes significant defects in longevity and climbing ability and causes bang sensitivity.

Vacuolization in *Pss* mutant brains

Vacuoles are frequently considered a histological hallmark of neurodegeneration in *Drosophila* (Fergestad et al., 2008; Palladino et al., 2002). To examine whether the *Pss* mutant's phenotypes stem from neurodegeneration in the CNS, we examined vacuole formation in 5-day-old brains of $Pss^{32/15}$ and wild-type flies. $Pss^{32/15}$ mutant brains contain many vacuoles (black arrowheads in Figure 2F a-h). After measuring the diameter of each vacuole by ImageJ, the total numbers of vacuoles with diameter from 3 μm to 6 μm and over 6μm in each fly brain were divided by the total number of slices of each fly brain to obtain the average number of vacuoles per plane (Figure 2F i). We frequently observed very large vacuoles in mutant flies (white arrows in Figure 2F c-g) but not in the wild-type flies (Figure 2F a-b). $Pss^{32/15}$ flies with *Actin-GAL4* and *UAS-Pss* are partially rescued as the number of vacuoles decreased significantly (Figure 2F i). On the basis of these observations, we conclude that *Pss* mutant brains exhibit hallmarks of neurodegeneration, which may underlie the behavioral phenotypes.

Defective mitochondria in *Pss* mutant flies

Mammalian PSS1 is commonly found in the membrane of the ER and is enriched in the MAM of ER contacts with the mitochondria (Stone and Vance, 2000). PS synthesized by PSS1 is translocated to the mitochondria, where it is converted into PE (Vance and Tasseva, 2013). Because PE is an important phospholipid for maintaining the stability of the mitochondrial inner membrane in mammals (Schenkel and Bakovic, 2014;

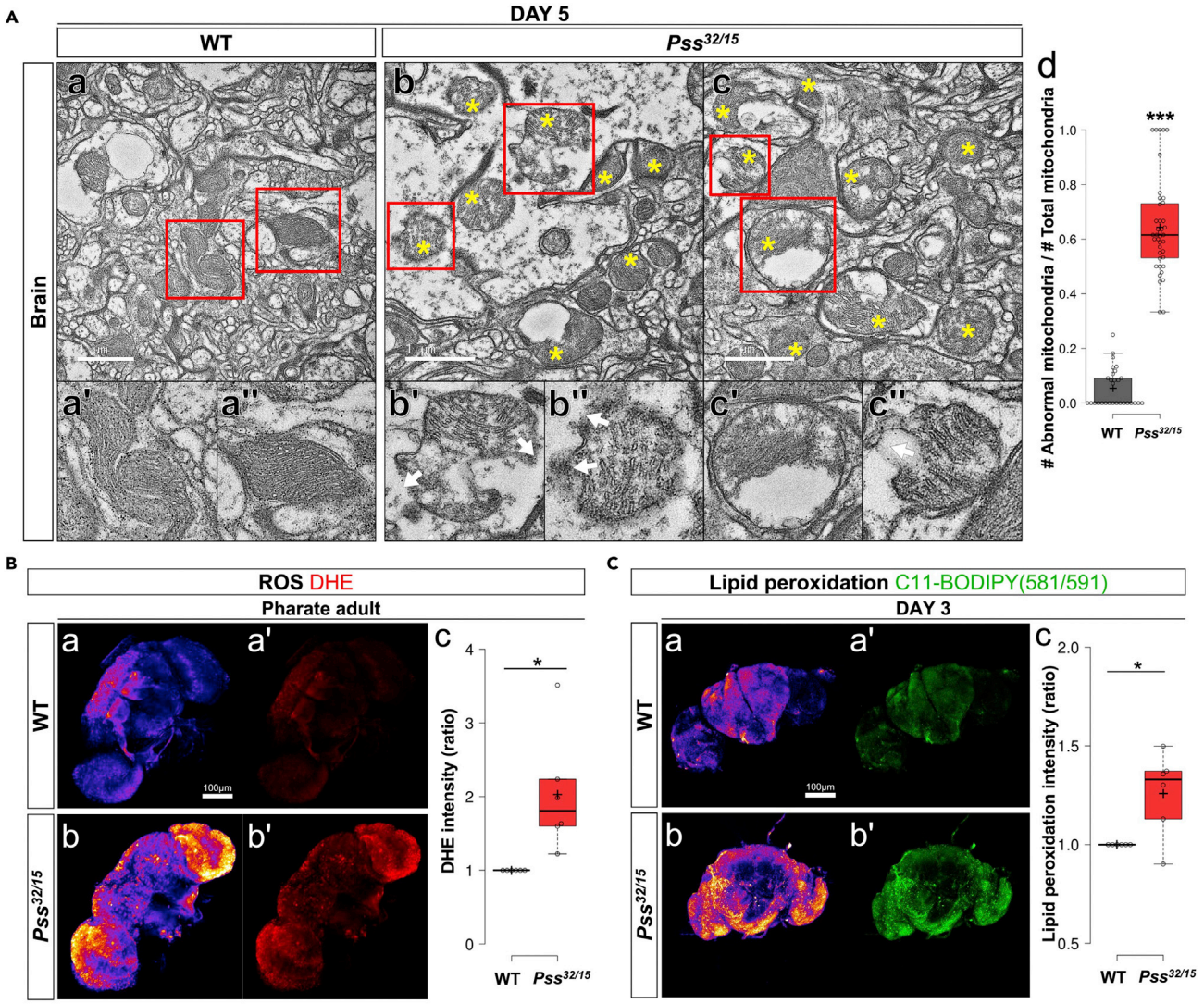

Figure 3. *Pss* mutation results in abnormal mitochondrial morphology and increased ROS production in the brain

(A) TEM images of mitochondria in the brain of 5-day-old (a) WT and (b-c) $Pss^{32/15}$ adults. (a-c) Areas indicated by red boxes in the upper panels are shown at higher magnification in the lower panels (a'-c', a''-c''). (a', a'') WT mitochondria were elliptical with orderly cristae structures. $Pss^{32/15}$ mitochondria have abnormal shapes (non-elliptical), sizes, and cristae patterns (defective mitochondria are indicated by yellow stars). (b', b'', c'') Occasionally, ruptured mitochondria are observed as indicated by white arrows, and (c') swollen mitochondria are also detected. Scale bar, 1 µm. (e) Quantification of abnormal mitochondria. Data points indicate the ratio of the 'number of abnormal mitochondria/number of total mitochondria' observed from the different TEM figures. ***$p < 0.001$.

(B) Detection of ROS in the brain with dihydroethidium (DHE). (a, a') Pharate adult WT. (b, b') Pharate adult $Pss^{32/15}$. Enhanced ROS production was found in the brain of *Pss* mutants. (a, b) Images are shown in 'fire' mode for better contrast. (c) Boxplots showing quantification of the DHE intensities. At least five specimens were measured for quantification. Scale bar, 100 µm. *$p < 0.05$.

(C) Detection of lipid peroxidation in the brains by C11-BODIPY(581/591). (a, a') 3-day-old WT. (b, b') 3-day-old $Pss^{32/15}$. (a, b) Images of the green fluorescent signals were converted to 'fire' modes for better contrast. (c) Boxplots showing quantified fluorescence intensities. At least five specimens were used for the quantification. Scale bar, 100 µm. *$p < 0.05$.

Tamura et al., 2012; Vance, 2014), we asked whether the mitochondrial inner membrane is compromised when *Pss* expression is reduced. We used transmission electron microscopy (TEM) to examine mitochondrial morphology in the brain and retina of 5-day-old $Pss^{32/15}$ mutants and wild-type flies. Mitochondria in the wild-type flies were, in general, elliptically shaped with orderly, tightly packed cristae (Figures 3A a, a', a'', and S2A a, a', a''). In contrast, the majority of mitochondria in $Pss^{32/15}$ flies were round in shape and appeared swollen or deformed (Figures 3A b-c, b'-c', b''-c'', d, and S2A b-c, b'-c', b''-c'', d). They also

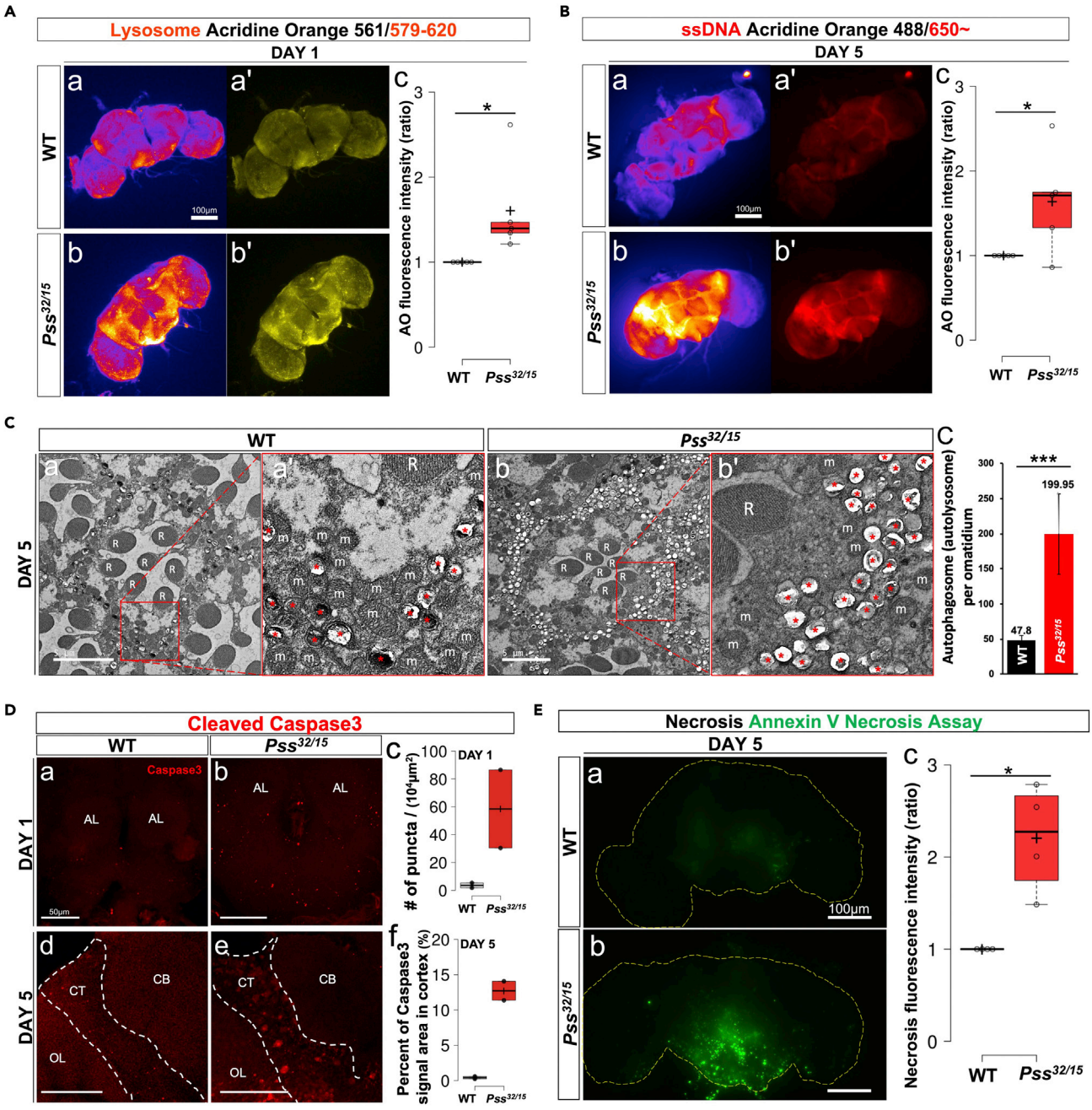

Figure 4. Increased autophagy, apoptosis, and secondary necrosis in *Pss* mutants

(A) Autophagy in the brain detected by acridine orange (AO) (excitation/emission: 561/579–620). (a, a') 1-day-old WT. (b, b') 1-day-old *Pss*$^{32/15}$. (a, b) Brain images are shown in 'fire' mode for better contrast. (c) Boxplots of quantified fluorescence intensities. At least five specimens were used for the quantification. Scale bar, 100 µm. *p < 0.05.

(B) Dying cells detected by AO in the brains. AO binding with ssDNA emits fluorescence at a longer wavelength than 650 nm (excitation: 488 nm). (a, a') 5-day-old WT. (b, b') 5-day-old *Pss*$^{32/15}$. (a, b) Brain images are shown in 'fire' mode for better contrast. (c) Boxplots of quantified fluorescence intensities. At least five specimens were used for the quantification. Scale bar, 100 µm. *p < 0.05.

(C) TEM images of ommatidia of (a) 5-day-old WT and (b) *Pss*$^{32/15}$ flies. The inter-ommatidial area that is composed of pigment cells is greatly expanded in *Pss*$^{32/15}$ flies. Red boxes in a, b are magnified in a', b'. R: rhabdomeres, m: mitochondria. Autophagic bodies are indicated by asterisks (*). (c) A bar graph showing numbers of autophagosomes/autolysosomes per ommatidium. *Pss*$^{32/15}$ flies display about 4.2 times more autophagosomes/autolysosomes per ommatidium than WT flies. Twenty specimens were used for the quantification. The error bars represent mean ± SD (***p < 0.001). The numbers above the error bars indicate mean values. Scale bar, 5 µm.

Figure 4. *Continued*

(D) Detection of apoptotic cells with anti-cleaved caspase 3 antibody. (a, d) WT. (b, e) *Pss*$^{32/+}$. (c) Boxplots of quantified immunofluorescent puncta per $10^4\mu m^2$ of 1-day-old flies' central brains ((total puncta number/area)x10^4). (f) Boxplots of quantified immunosignal area in cortex of 5-day-old flies' brains ((signal positive area/total cortex area)x100). AL: antennal lobe, CB: central brain, CT: cortex, OL: optic lobe. Scale bar, 50 μm.

(E) Secondary necrosis in *Pss* mutants. WT and *Pss*$^{32/15}$ brains were stained with a necrosis detector. (a) While only faint signals appeared in the WT brains, (b) strong and widespread signals appeared in the mutant brains. (c) Boxplots of quantified fluorescence intensities. At least four specimens were used for the quantification. Scale bar, 100 μm. *$p < 0.05$.

displayed irregular cristae structures and ruptured membranes (white arrows in Figures 3A b', b'', c'', and S2A b'-c', b''-c''). Such structural deformities suggest that reduced PS production due to reduced *Pss* expression undermines the stability of the mitochondrial inner membrane, leading to disorganized cristae, swelling, and rupture.

Elevation of ROS in *Pss* mutant flies

Reactive oxygen species (ROS) are produced mostly by complex I in mitochondria, and healthy mitochondria contain enzymatic mechanisms to lower ROS levels (Starkov, 2008). Since elevated levels of oxidative stress are known to be a major cause of neurodegeneration (Sies, 2017), we hypothesized that the abnormal mitochondrial structure in *Pss* mutants may be associated with a systemic increase in ROS levels in the brain. To determine whether this is the case, we measured ROS levels in the brains of both *Pss* mutant and wild-type flies using red fluorescence emitted by dihydroethidium (DHE) in response to ROS (Owusu-Ansah et al., 2008).

Since *Pss*$^{32/15}$ mutants showed behavioral defects in young adults (Figures 2C–2E), we measured ROS levels in late pupal brains. Pharate adult brains of *Pss*$^{32/15}$ mutants exhibit significantly higher levels of red fluorescence than wild-type brains (Figure 3B). Because the ND phenotype presents later in heterozygotes than in the *trans*-heterozygotes, we examined the aging effect in the heterozygotes by measuring ROS levels in brains of older *Pss*$^{32/+}$ flies. 5-day-old *Pss*$^{32/+}$ flies had higher levels of red fluorescence than 5-day-old wild-type flies (Figure S2B). These results suggest that reduced *Pss* expression increases ROS levels.

Lipids, especially polyunsaturated fatty acid (PUFA), are more susceptible to oxidation in the presence of ROS. Thus, lipid peroxidation products can be used as a biomarker for *in vivo* oxidative stress (Abuja and Albertini, 2001). We measured lipid peroxidation by staining brains with C11-BODIPY(581/591) in 3-day-old wild-type and *Pss*$^{32/15}$ flies. As shown in Figure 3C, lipid peroxidation was significantly higher in mutant brains than in wild-type brains. We also found increased lipid peroxidation in the brains of 10-day-old *Pss*$^{32/+}$ flies relative to wild-type flies (Figure S2C). On the basis of these data, we suggest that mitochondrial dysfunction in *Pss* mutant flies is associated with increased ROS production in the brain.

Increased autophagic activity in the brain and retina of *Pss* mutants

The data presented above show that the majority of mitochondria in the brain and retina of *Pss*$^{32/15}$ mutants are abnormally shaped (Figures 3A and S2A). Since autophagy is an important mechanism for removing dysfunctional organelles (Mizushima, 2007), we wondered whether the autophagic activity was also affected by *Pss* mutation. Acridine orange (AO) is a lysotropic dye that is protonated at acidic pH and trapped in acidic vesicular organelles such as autophagosomes/autolysosomes. Hence, red fluorescence of 579–620 nm emitted from AO with excitation at 561 nm can be used to detect cellular autophagic activity (Thome et al., 2016). We stained 1-day-old brains from *Pss*$^{32/15}$, and wild-type flies with AO. Brains from *Pss*$^{32/15}$ flies showed strong fluorescent signals (Figure 4A). We also examined autophagic activities in *Pss*$^{32/+}$ flies to assess whether aging also affects autophagic activity. Notably, in contrast to the *Pss*$^{32/15}$ flies, there was no significant difference in fluorescence between the 1-day-old *Pss*$^{32/+}$ and wild-type flies; however, 10-day-old *Pss*$^{32/+}$ flies showed high levels of red fluorescence (Figure S2D). These results suggest that even heterozygous *Pss*$^{32/+}$ flies display higher levels of autophagic activity upon aging.

To gain further histological evidence for enhanced autophagy in *Pss* mutants, we processed sections of the compound eyes for TEM to examine autophagosome/autolysosome structures in retinal pigment cells, a type of glial cell (Edwards and Meinertzhagen, 2010). To our surprise, the inter-ommatidial area where retinal pigment cells are located was atypically broad in *Pss*$^{32/15}$ flies (Figure 4C a vs. b). Moreover, we observed numerous dark and white bodies enclosed by a double lipid bilayer, characteristic of autophagosomes/autolysosomes (Eskelinen et al., 2011) and *Pss* mutants contained more autophagosomes than

A

	da-GAL4	Pss-GAL4	repo-GAL4	elav-GAL4
Pss RNAi with Dcr2	Lethal (before 3rd instar larvae)	Lethal (before 3rd instar larvae)	Lethal (pupal stage)	Viable

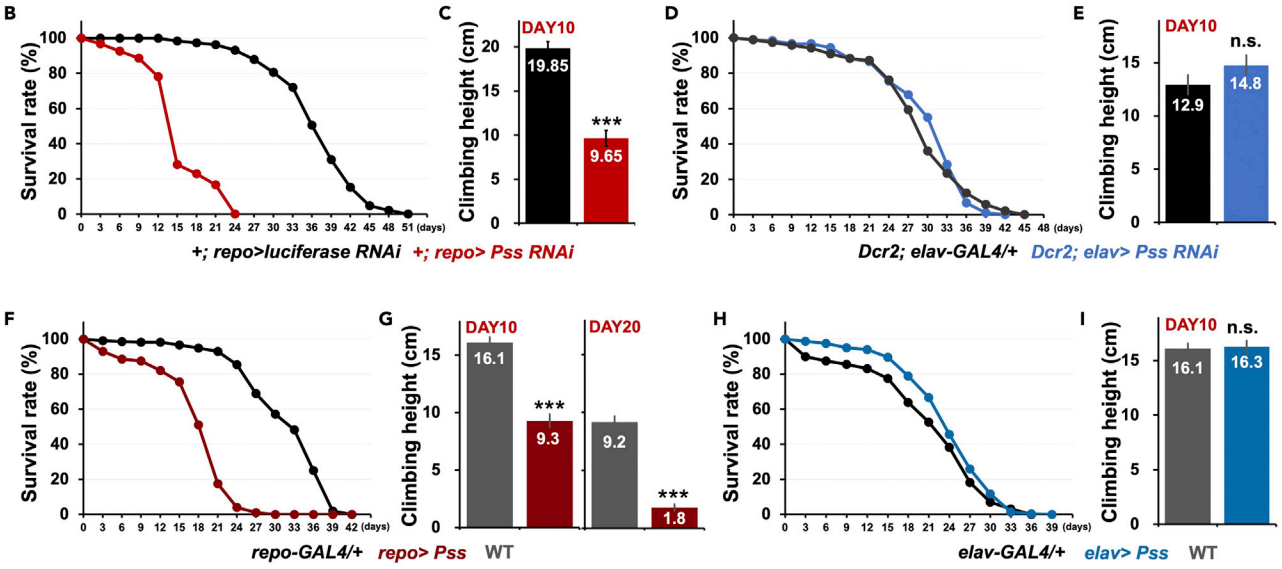

J

	Cortex glia (NP2222-GAL4)	Perineurial glia (NP6293-GAL4)	Subperineurial glia (NP2276-GAL4)	Astrocyte-like glia (alrm-Gal4)	Wrapping glia (Mz97-Gal4)
Pss RNAi with Dcr2	Semi-lethal (viability 37%, 54/144.5)	Delayed development	Viable	Viable	Viable

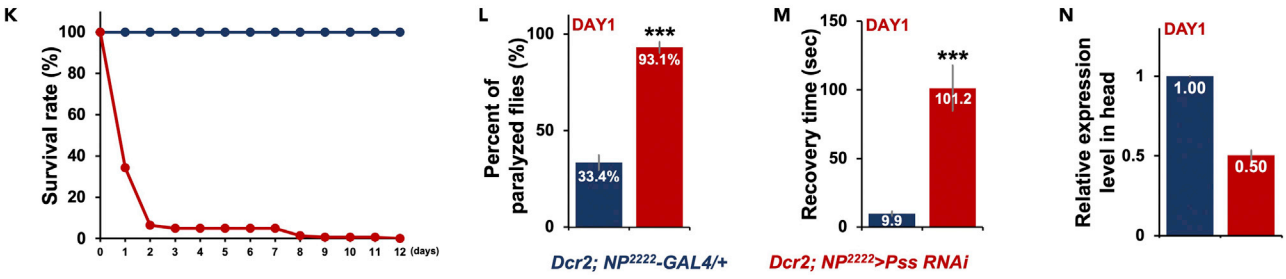

Figure 5. Glia-specific functions of *Pss*

(A) *Pss RNAi* expression with *Dcr2* by *da-GAL4*, *Pss-GAL4*, or *repo-GAL4* caused lethality, whereas knockdown by neuron-specific *elav-GAL4* produced viable adults without any noticeable defects.

(B and C) Escapers of Pan-glial *Pss* knockdown without *Dcr2* (*+; repo>Pss RNAi*) produced a significant reduction in life span and climbing ability. (B) life span, control n = 190, *+; repo>Pss RNAi* n = 96 (Log rank test: $p < 0.0001$). (C) Climbing behavior was analyzed in 10-day-old flies. control n = 77, *+; repo>Pss RNAi* n = 52. Bars represent the mean ± SEM. ***$p < 0.001$. Numbers within bars indicate mean values.

(D and E) Pan-neuronal *Pss* knockdown (*Dcr2; elav>Pss RNAi*) does not obviously affect development, longevity, and climbing ability. (D) life span, control n = 189, *Dcr2; elav>Pss RNAi* n = 180 (Log rank test: $p = 0.7291$). (E) Climbing behavior was analyzed in 10-day-old flies. control n = 40, *Dcr2; elav>Pss RNAi* n = 40. Bars represent the mean ± SEM. n.s., not significant. Numbers within bars indicate mean values.

(F and G) Pan-glial *Pss* overexpression (*repo>Pss*) does not affect development but leads to a significant reduction in life span and climbing ability. (F) life span, control n = 212, *repo>Pss* n = 200 (Log rank test: $p < 0.0001$). (G) Climbing behavior was analyzed in 10- and 20-day-old flies. WT n = 100, *repo>Pss* n = 100. Bars represent the mean ± SEM. ***$p < 0.001$. Numbers within bars indicate mean values.

(H and I) Pan-neuronal *Pss* overexpression did not affect development, longevity, and climbing ability. (H) life span, control n = 160, *Dcr2; elav>Pss RNAi* n = 366 (Log rank test: $p = 0.0157$). (I) Climbing behavior was analyzed in 10-day-old flies. WT n = 100, *+; repo>Pss RNAi* n = 100. Bars represent the mean ± SEM. n.s., not significant. Numbers within bars indicate mean values.

(J) Lethality caused by glia subtype-specific *Pss* knockdown.

Figure 5. *Continued*

(K) Survival rate of cortex glia-specific *Pss* knockdown (*Dcr2; NP2222>Pss RNAi*) mutants. Most died within 48 hr at 29°C. control n = 150, *Dcr2; NP2222>Pss RNAi* n = 140 (Log rank test: $p < 0.0001$).

(L and M) Bang-sensitive phenotypes of 1-day-old flies. (L) Cortex glia *Pss* knockdown (*Dcr2; NP2222>PssRNAi*) mutants (n = 94) were much more sensitive to shock than the control flies (n = 122). (M) Recovery time for paralyzed flies. *Pss* mutant flies took longer to recover. Bars represent the mean ± SEM. ***$p < 0.001$.

(N) Relative *Pss* expression level in the head of cortex glia-specific knockdown flies and control flies. Bars represent max and min values.

wild-type flies (Figure 4C). These results provide further support for increased autophagic activity in *Pss* mutant flies, likely to remove dysfunctional mitochondria.

Loss of *Pss* leads to enhanced cell death and secondary necrosis in the CNS

We wondered whether vacuole formation in the brain of $Pss^{32/15}$ mutants was due to excessive cell death caused by the increased number of dysfunctional mitochondria and/or by elevated oxidative stress induced by high levels of ROS. Both have been implicated in cell death (Gaschler and Stockwell, 2017). Deep red fluorescent signals (longer than 650 nm) from AO after excitation at 488 nm can be used to detect dying cells (Sarkissian et al., 2014). Hence, we examined deep red fluorescent signals in AO-treated brain tissue from 5-day-old $Pss^{32/15}$ and wild-type flies. We observed weak fluorescent signals in various parts of the wild-type brain (Figures 4B a, a'). By comparison, the signals were much more intense in $Pss^{32/15}$ mutants (Figures 4B b, b', c). Similar results were obtained for 20-day-old $Pss^{32/+}$ (Figure S2E) flies. Together, these results show enhanced cell death in *Pss* mutant brains.

To determine if cell death in *Pss* mutants is caused by caspase-mediated apoptosis, brain samples were stained for caspase 3 (anti-cleaved caspase 3). Since this antibody reacts selectively with activated effector caspases in *Drosophila*, it is commonly used to detect apoptotic cells. We detected immunofluorescent puncta throughout the central brain of 1-day-old $Pss^{32/15}$ flies, more than in 1-day-old wild-type flies (Figure 4D a-c). Notably, more prominent immunosignal was detected in 5-day-old $Pss^{32/15}$ brains (Figure 4D e). These signals appeared to be more concentrated in the cortex (CT), whereas such signals were rarely observed in similarly aged wild-type flies (Figure 4D d-f). We propose that enhanced autophagy and apoptosis are both causally associated with the neurodegenerative phenotype observed in *Pss* mutant brains.

Necrotic cell death is also associated with PS. PS is involved in the clearance of apoptotic cells by acting as an eat-me signal that is recognized by scavenging cells (Segawa and Nagata, 2015). The absence or reduction of phagocytic clearance due to reduced PS signals results in the autolysis of apoptotic cells termed secondary necrosis (Silva, 2010). Cytoplasmic contents, including lysosomal enzymes and ROS that are released from autolyzed apoptotic cells, further damage surrounding cells, eventually killing them (Muñoz et al., 2010). Because *Pss* mutants contain a reduced amount of PS, we hypothesized that secondary necrosis might occur more frequently in mutants than in wild-type flies. To test this hypothesis, wild-type and $Pss^{32/15}$ brains were stained with a necrosis detector, which emits green fluorescence only when it enters necrotic cells. Indeed, we detected either no signals or very faint signals in wild-type brains at both 5 days (Figure 4E a) and 10 days old (Figure S2F a). However, 5-day-old $Pss^{32/15}$ mutants showed strong, widespread signals (Figures 4E b, c) that increased further in 10-day-old flies (Figure S2F b). These results indicate that *Pss* mutation led to secondary necrosis in the brain tissue, which is accelerated with aging.

Glia-specific function of *Pss*

To further investigate *Pss*'s function, we employed an RNAi-mediated silencing tool (*Pss-RNAi*). Ubiquitous knockdown of *Pss* expression by *da-GAL4* caused developmental arrest at early larval stages (Figure 5A). *da>Pss RNAi* embryos hatched into first instar larvae but died before reaching the third instar larval stage. *Pss* knockdown using *Pss-GAL4* showed the same results as *da-GAL4*. The larval lethality phenotype, when compared with the embryonic lethality of homozygous *Pss* mutants, likely reflects the hypomorphic nature of *RNAi*-mediated knockdown. Nevertheless, these results further indicate that *Pss* plays a vital role in both embryonic and larval development.

Reporter expression driven by *Pss-GAL4* was highly enriched in subsets of the glial population in the CNS (Figure 1E). We found that the pan-glial knockdown of *Pss* (*repo>Pss RNAi*) resulted in pupal lethality (Figure 5A). However, the pan-neuronal knockdown of *Pss* (*elav>Pss RNAi*) did not produce any noticeable

defects either during development or in adults (Figures 5A, 5D, and 5E). Together, these results suggest that glial-specific *Pss* expression appears to be essential for pupal development.

As we did not observe any adult flies from *repo>Pss RNAi* developed in 25°C, we generated milder knockdowns in flies by raising the flies expressing *repo>Pss RNAi* without *Dcr2* at 22°C during development. The escapers (+; *repo>Pss RNAi*) showed a dramatically decreased life span (T50, 15 days) compared with control flies (T50, 37.2 days) (Figure 5B). They also exhibit climbing defects at day 10 when compared with the control flies (Figure 5C).

Furthermore, to eliminate the effects of *Pss* knockdown during development and to assess if pan-glial knockdown of *Pss* after eclosion can also cause neurodegeneration, we used the temperature-sensitive GAL80^{ts}, which provides a temporal regulation of UAS transgene by preventing GAL4-dependent transcription (Duffy, 2002). As a result, *+; tubGAL80; repo>Pss RNAi* flies (T50, 33.5 days) and *Dcr2; tubGAL80; repo>Pss RNAi* flies (T50, 28 days) have a decreased life span compared with the control flies (T50, 42.5 days) (Figure S3A). In the climbing assay, both mutant flies did not show any significant difference compared with the control flies at day 10 (Figure S3B). However, mutant flies showed severe climbing defects when aged for 30 days (Figure S3C). These results strongly support that glial-specific *Pss* is also essential for the maintenance of the nervous system in adults.

Given *Act>Pss; Pss$^{32/15}$* flies partially rescued the *Pss$^{32/15}$* but still displayed a relatively shorter life span than wild-type flies (Figure 2B), we examined whether overexpression of *Pss* has any deleterious effects. Adult flies carrying ectopic *Pss* expression in pan-neuronal cells (*elav>Pss*) developed normally and did not show any noticeable changes in life span or climbing, suggesting that neuronal cells were not affected by the elevated *Pss* expression (Figures 5H and 5I). Moreover, Pan-glial overexpression of *Pss* (*repo>Pss*) did not grossly alter either embryonic or postembryonic development. However, these adults had a significantly reduced life span (T50, 19.8 days) compared with controls (T50, 31.8 days) (Figure 5F) and exhibited reduced climbing ability: a 42% reduction at 10 days old and an 80% reduction at 20 days (Figure 5G). Even wild-type flies showed an approximately 2-fold reduction in climbing height when aged 10 days old or more, suggesting that aging affects this behavior. Nonetheless, our results show that climbing performance deteriorated more precipitously with aging in *repo>Pss* flies. On the basis of these results, we speculated that pan-glial overexpression of *Pss* accelerates aging-associated neurodegeneration. In line with this, we found more vacuoles in the brains of *repo>Pss* flies, whereas wild-type brains were relatively well-shaped with fewer vacuoles (Figure S3D).

To assess if *repo>Pss* also increases apoptosis of glial cells, we co-labeled the brains of 15-day-old *repo>Pss* flies with anti-cleaved caspase 3 and anti-Repo. Although controls (*repo-GAL4/+*) showed little caspase 3 immunoreactivity, *repo>Pss* flies had higher levels of immunoreactivity throughout the brain, as well as dense label in some small areas (Figure S3E a vs. b), anti-Repo signals are limited to the nucleus, and anti-cleaved caspase 3 immunoreactive signals are seen mainly in the cytoplasm. As shown in magnified images (Figure S3E b'), we observed high levels of anti-cleaved caspase 3 immunosignals surrounding Repo-expressing nuclei, as well as in some cells lacking Repo expression, suggesting that cell death events were taking place in glial cells, as well as in neuronal cells. Since both pan-glial knockdown and overexpression of *Pss* led to defects indicative of neurodegeneration, we speculate that glial *Pss* expression must be tightly regulated to maintain the adult CNS.

To determine the glial subtype(s) that require *Pss* function, *GAL4* drivers specific to each glial subtype were used to knockdown *Pss* expression: *NP2222-GAL4* (cortex glia), *NP6293-GAL4* (perineurial glia), *NP2276-GAL4* (subperineurial glia), *Alrm-GAL4* (astrocyte-like glia), and *Mz97-GAL4* (wrapping glia). Each *GAL4* line was crossed to *UAS-RNAi-Pss* expressing *Dcr2*, and the offspring were examined for developmental defects (Figure 5J). Interestingly, knockdown of *Pss* in the cortex glial subtype (*Dcr2; NP2222>Pss-RNAi*) produced semi-lethality during pupal development and only 37.4% of expected flies eclosed. Knockdown of *Pss* in perineurial glia (*Dcr2; NP6293>Pss-RNAi*) produced delayed development. *Pss* knockdown in the other glial subtypes did not produce any noticeable defects. From these results, we infer that both cortex and perineurial glia require *Pss* and that *Pss* expression in these glial subtypes is required for normal development.

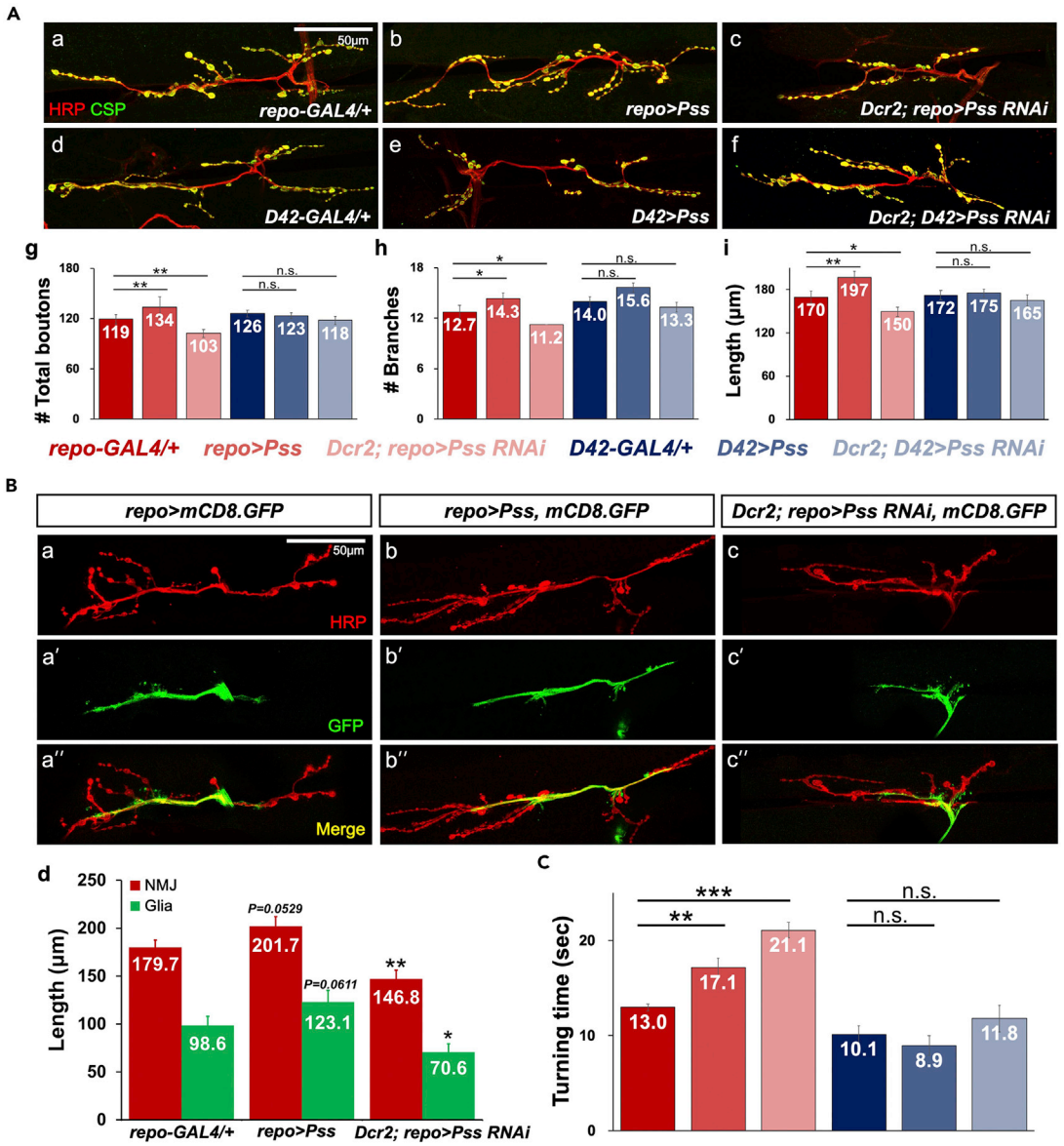

Figure 6. *Pss* expression alters synaptogenesis and axonal development in larval motoneurons and larval behavior

NMJ morphology was assessed in the sixth and seventh muscles in the third abdominal segment of third-instar larvae.

(A) NMJ structures affected by mutations and overexpression of *Pss* in a glial-specific manner. (a-f) Merged images of HRP immunostaining for the neuronal membrane (red) and CSP immunostaining for pre-synaptic vesicles (green) are shown for the genotypes indicated in each panel. Overexpression and knockdown of *Pss* were achieved by *repo-GAL4* in glial cells and by *D42-GAL4* in larval motoneurons. Scale bar, 50 μm. (g-i) Quantitative analysis of (g) bouton numbers, (h) axonal branches, and (i) NMJ length. Each genotype was color-coded, as indicated below the graphs. At least 17 specimens were assessed for each genotype. *p < 0.05; **p < 0.01; n.s., not significant.

(B) Effect of pan-glial overexpression (*repo>Pss*) and knockdown of *Pss* (*Dcr2; repo>Pss RNAi*) on the growth of glial processes and NMJ length. *repo>mCD8.GFP* was used as a marker of the glial cell membrane. (a-c) HRP immunostaining (red), (a′-c′) mCD8.GFP expression (green), and (a"-c") merged pictures of both labelings. Scale bar, 50 μm. (d) A histogram showing the average lengths of NMJs and glial processes affected by glial-specific overexpression and knockdown of *Pss*. At least 14 specimens were observed for each genotype. Bars represent the mean ± SEM values. *p < 0.05; **p < 0.01.

(C) Larval roll-over assay. Larvae carrying glial-specific knockdown or overexpression of *Pss* take significantly longer to roll over. Bar colors for the genotypes are the same as in (A). At least 20 larvae were tested for each genotype. Bars represent the mean ± SEM values. *p < 0.05; **p < 0.01; ***p < 0.001; n.s., not significant.

Because of the observed developmental defect, we investigated the phenotype of *Dcr2; NP2222>Pss-RNAi* further. Intriguingly, most of the adults carrying *Dcr2; NP2222>Pss-RNAi* died within 48 hr when grown at 29°C (Figure 5K). They also showed significantly increased bang sensitivity: shock-induced paralysis was observed in 93.1% of 1-day-old flies, but only 33.4% of control flies (Figure 5L). These flies also took 101.2 s on average to recover from shock-induced paralysis, whereas control flies took 9.9 s (Figure 5M). We performed qRT-PCR using heads extracts and observed a 50% reduction in *Pss* transcripts in the cortex glia specific knockdown flies (Figure 5N). This is a significant change considering that the heads extracts include numerous other cell types, and cortex glia only correspond to about to a few % of the number of neurons and glia in adult brains. These results suggest that *Pss* expression in cortex glia is essential for pupal development and adult CNS function.

Glia-specific *Pss* functions are important for the synaptogenesis of larval motoneurons

Glial cells play an essential role in synaptic formation and differentiation (Ullian et al., 2004). For example, glial cells are known to regulate the growth of synapses in the larval neuromuscular junction (NMJ) (Brink et al., 2012). Because the previous data suggest an essential role of proper *Pss* expression in glial cells, we investigated whether *Pss* is also important for NMJ synapse development in larvae. NMJs were stained with anti-HRP antibody (red) to label the neuronal membrane and anti-CSP antibody (green) to visualize presynaptic vesicles (Brent et al., 2009). We counted synaptic boutons and branches, and measured the NMJ length for muscles 6/7 of the third abdominal segment (Figure 6A). Glia-specific knockdown (*Dcr2; repo>RNAi-Pss*) resulted in a significant reduction in the number of boutons and branches and NMJ length when compared with controls (Figure 6A a, c, and g–i). Conversely, ectopic *Pss* expression in glial cells (*repo>Pss*) enhanced synaptogenesis, as indicated by increased numbers of boutons and branches (Figures 6A a, b, and g–i). By contrast, neither knockdown nor overexpression of *Pss* in the larval motoneurons using *D42-GAL4* (*Dcr2; D42>RNAi-Pss* and *D42>Pss*) had any significant effect on synaptogenesis (Figures 6A d–f, and g–i). These results further suggest that glia-specific *Pss* functions are required for optimal synaptogenesis at the larval NMJ.

To assess if the development of glial is affected by abnormal levels of *Pss* expression, we measured the lengths of the NMJs and glial processes (Figure 6B). Glial processes were labeled with membrane-tethered mCD8.GFP driven by *repo-GAL4*, and motoneuronal axon membranes were counterstained with anti-HRP. We found that both glial process length and distal axon length (also termed the NMJ length) were indeed correlated with *Pss* levels, whereas *repo>Pss* produced an increase in the length of both NMJs and glial processes when compared with *repo-GAL4/+* control (Figure 6B a, b, and d), and the opposite was observed with *Pss* knockdown (Figure 6B c, and d). From these data, we conclude that glia-specific *Pss* functions are required for the optimal growth of glial processes that guide axonal growth and synaptogenesis of motor neurons.

It is possible that both subnormal and excessive synaptogenesis of motoneurons affect larval motor skills. To test this, we performed roll-over assays in which we inverted a larva so that the ventral side is facing up and measured the time the larva to recover to their normal posture. Indeed, larvae with either glial knockdown (*Dcr2; repo>Pss-RNAi*) or overexpression (*repo>Pss*) of *Pss* took significantly longer to recover than control larvae (Figure 6C). Meanwhile, the same transgenic manipulations in motoneurons driven by *D42-GAL4* produced no significant deficits in the roll-over assay (Figure 6C). These data suggest that abnormal synaptogenesis at NMJs resulting from altered expression of *Pss* in glial cells impairs the function of larval motoneurons. These results further support the hypothesis that the expression levels of *Pss* in glial cells must be tightly regulated.

DISCUSSION

Changes in phospholipid levels have been reported in the brains of patients with neurodegeneration, such as AD and PD (Li et al., 2015; Pettegrew et al., 2001). However, it has not yet been determined whether changes in phospholipid levels are sufficient to lead to NDs. In this study, we demonstrate that loss of *Pss* and overexpression of the *Pss* gene encoding a *Drosophila* homolog of mammalian PSS1 and 2 cause severe neurodegenerative phenotypes. These flies display defects in longevity, climbing ability, and bang sensitivity. We further document the formation of numerous vacuoles in brains with reduced *Pss*. Finally, we showed that either glia-specific knockdown or overexpression of *Pss* is sufficient to induce neurodegenerative features (Figure 5) in aging flies. We argue that the level of PSS is critical and needs to be properly controlled.

PS is one of the major substrates for the production of PE, which is critical for the stability of the mitochondrial inner membrane (Schenkel and Bakovic, 2014; Tamura et al., 2012; Vance, 2014). A decrease in mitochondrial PE impairs cell growth, respiratory capacity, and ATP production and profoundly alters mitochondrial morphology in mammalian cells (Tasseva et al., 2013). Also, reduction of PE production in mitochondria causes fragmented, misshapen mitochondria in mice (Steenbergen et al., 2005). A recent study has shown that the level of PS in salivary gland is dramatically reduced in salivary gland-specific *Pss RNAi* flies to around 20% of control flies (Yang et al., 2019). Hence, reduced PS synthesis in our *Pss* mutants may affect PE production in mitochondria, which in turn affects mitochondrial structure and function. This is consistent with our observation of a large population of swollen and ruptured mitochondria with disorganized cristae in *Pss* mutant. Abnormal and dysfunctional mitochondria are removed by autophagy because ruptured mitochondria release excessive ROS to the cytoplasm (Thomas and Gustafsson, 2013). Increases in either cytoplasmic ROS levels or the number of dysfunctional mitochondria will eventually kill affected cells (Bhat et al., 2015; Jena, 2012). Indeed, *Pss* mutants had a large population of misshapen and ruptured mitochondria, higher ROS levels, and increased cell death by both autophagy and apoptosis. Therefore, the neurodegeneration observed in *Pss* mutants may be a consequence of mitochondrial dysfunction.

PS has also been well recognized as an "eat-me" signal for phagocytic clearance of apoptotic cells (Fadok et al., 1992; Leventis and Grinstein, 2010; Segawa and Nagata, 2015), and PS exposure is necessary for detection by phagocytes (Borisenko et al., 2003; Fadok et al., 2001). Phagocytosis is a vital component in the development and homeostasis of neural tissue, and the abnormal phagocytic ability has been linked to many diseases (Napoli and Neumann, 2009; Poon et al., 2014; Ravichandran, 2011; Salter and Stevens, 2017; Von Bernhardi et al., 2015; White and Gallin, 1986). Also, the absence of the phagocytic receptor *Draper (drpr)* in glia leads to a pronounced accumulation of apoptotic neurons in the brain of *Drosophila* (Etchegaray et al., 2016). *Pss* mutants are expected to have lower external PS levels but increased cell death events. Recent studies have shown that if apoptotic cells are not properly removed, the cells will eventually autolyze (secondary necrosis), releasing cytotoxic substances and killing exposed neighboring cells (Muñoz et al., 2010). Therefore, increased cell death in the *Pss* mutant brain may be due to secondary necrosis. Indeed, *Pss* mutants showed a strong increase in necrotic signals. Therefore, the primary apoptosis can be initiated by mitochondrial defect, but the reduction of phagocytic clearance and the secondary necrosis should accelerate the neurodegeneration in the *Pss* mutants and may even have a primary role.

Glia are non-neuronal cells that play an essential role in the trophic support of neurons, regulation of neuronal morphology, extracellular homeostasis, establishment of the blood-brain barrier, myelination, and axon growth and guidance (Chotard and Salecker, 2007; Liu et al., 2015), and abnormal glial function is associated with many NDs (Chung et al., 2020; Lee and Sun, 2015). Interestingly, we found that *Pss* is mostly expressed in a subset of glia in the CNS, and glia-specific knockdown or overexpression of *Pss* altered synaptogenesis and axonal growth in larval motoneurons. Moreover, glia-specific knockdown of *Pss* caused reduced life span and climbing defect. Importantly, the glial knockdown of *Pss* specifically after eclosion using the Gal80 system induces neurodegeneration as the flies aged. These results indicate that *Pss* is essential for glia not only during developmental stages but also for the maintenance of the nervous system in the adult. Furthermore, glia-specific overexpression of *Pss* also resulted in neurodegenerative phenotypes in the adult brain, and *trans*-heterozygous mutants in which *UAS-Pss* is expressed also showed reduction of life span and climbing ability compared with the wild-type flies due to the excessive expression of *Pss*, suggesting that *Pss* expression levels must be tightly regulated to maintain a healthy nervous system. In a recent study, increased expression of phagocytic receptors, SIMU or Drpr, in glia causes neuronal loss, motor defects, and early onset death, and these phenotypes are reversed by driving MFG-E8, which specifically binds PS and prevent the interaction between PS and the receptors (Hakim-Mishnaevski et al., 2019). In this context, overexpression of *Pss* is expected to increase the level and exposure of the PS in the plasma membrane, which may lead to excessive phagocytosis, resulting in neurodegeneration.

Recent studies emphasize the role of the lipid metabolism enzymes in glial cells (Chung et al., 2020; Griffin and Ackerman, 2020). One of the enzymes of the very-long-chain fatty acid (VLCFA) β-oxidation pathway in peroxisomes, ACOX1 (acyl-CoA oxidase 1), is mostly expressed and required in glia and both loss and gain of ACOX1 lead to glial degeneration. Moreover, another study indicates that elevated VLCFA levels can induce PS exposure on cell surfaces (Gong et al., 2017). Therefore, it will be interesting to test whether the PS containing VLCFA may also have important roles in glial cells.

There are six glial subtypes in *Drosophila* — cortex glia, ensheathing glia, astrocyte, perineurial glia, subperineurial glia, and wrapping glia — characterized in large part by their morphology and association with neurons (Freeman, 2015). Our genetic data suggest that *Pss* functions in cortex glia. Specific knockdown of *Pss* in cortex glia led to semi-lethality, a severely reduced life span as well as a significant increase in bang sensitivity, suggesting a crucial role for *Pss* in cortex glia. Cortex glia surrounds and supports neuronal cell bodies and the proximal regions of neurites as they extend toward the neuropil (Awasaki and Lee, 2011). Despite their notable morphology, cortex glial cells are the least well-characterized glial subtypes of the *Drosophila* CNS (Freeman, 2015), and further studies will be needed to clarify the functional relationships between *Pss* and cortex glia.

PSS seems to be essential not only for the maintenance of the nervous system but also for overall development. In humans, mutations in *PTDSS1* cause LMHD (MIM 151050), a rare disease which shows developmental defects, severe growth retardation, and intellectual disability. Overexpression of mutant *PTDSS1* RNA in zebrafish embryos also disrupts normal development (Sousa et al., 2014). *PSS1* and *PSS2* double knockout mice are prenatally lethal (Arikketh et al., 2008). These results and our observations suggest that *Phosphatidylserine synthase* plays a vital role in development, and further studies are necessary in order to uncover the specific role of these proteins in developmental processes.

In summary, our studies in *Drosophila* show that PSS is required for neuronal maintenance, and its loss or gain may cause NDs triggered by defective PS metabolism. Abnormal PS production in glial cells may have deleterious effects on the nervous system, including its development, maintenance, and/or function. We propose that changes in phospholipid composition, due mainly to abnormal levels of PS, are a cause of neurodegeneration rather than merely a consequence of disease.

STAR★METHODS

Detailed methods are provided in the online version of this paper and include the following:

- KEY RESOURCES TABLE
- RESOURCE AVAILABILITY
  - Lead contact and materials availability
  - Data and code availability
- EXPERIMENTAL MODEL AND SUBJECT DETAILS
  - Drosophila melanogaster strains
- METHOD DETAILS
  - Generation of Pss^{41} and *UAS-Pss*
  - Protein homology and alignment of *Pss*
  - Quantitative real-time PCR
  - Longevity, climbing ability, and bang sensitivity
  - Detection of vacuoles in the brain
  - NMJ analyses and larval roll-over assay
  - Immunohistochemistry
  - Detection of ROS in brain tissue
  - Detection of cell death in brain tissue
  - Transmission electron microscopy
  - Detection of necrosis
- QUANTIFICATION AND STATISTICAL ANALYSIS

SUPPLEMENTAL INFORMATION

Supplemental information can be found online at https://doi.org/10.1016/j.isci.2021.102899.

ACKNOWLEDGMENTS

This work was supported by the National Research Foundation of Korea Grant (NRF-2015R1D1A1A01059861, NRF-2019R1F1A1061772) to S.H.J. H.J.B. is an Investigator of the Howard Hughes Medical Institute. H.-L.C. is supported by the Warren Alpert Foundation. We appreciate the technical support of the Korea Basic Science Institute (KBSI), Chuncheon Center, and Seoul Center.

AUTHOR CONTRIBUTIONS

Y.-J.P., S.K., H.-P.S., H.-L.C., H.J.B., and S.-H.J. designed the experiments and wrote the manuscript. Y.-J.P., S.K., H.-P.S., T.-Y.K., M.-C.J., M.L, S.L., and J.Y. conducted experiments. A.-Y.K. generated the CRISPR/Cas9 mutation. J.H.P. and G.L. produced the *UAS-Pss* lines and wrote the manuscript. S.-H.K. conducted the analysis of confocal microscopy images.

DECLARATION OF INTERESTS

The authors declare no competing interests.

Received: April 21, 2021
Revised: June 14, 2021
Accepted: July 21, 2021
Published: August 20, 2021

REFERENCES

Abuja, P.M., and Albertini, R. (2001). Methods for monitoring oxidative stress, lipid peroxidation and oxidation resistance of lipoproteins. Clinica Chim. Acta Int. J. Clin. Chem. *306*, 1–17.

Arikketh, D., Nelson, R., and Vance, J.E. (2008). Defining the importance of phosphatidylserine synthase-1 (PSS1): unexpected viability of PSS1-deficient mice. J. Biol. Chem. *283*, 12888–12897.

Awasaki, T., and Lee, T. (2011). New tools for the analysis of glial cell biology in Drosophila. Glia *59*, 1377–1386.

Bellen, H.J., Levis, R.W., He, Y., Carlson, J.W., Evans-Holm, M., Bae, E., Kim, J., Metaxakis, A., Savakis, C., Schulze, K.L., et al. (2011). The Drosophila gene disruption project: progress using transposons with distinctive site specificities. Genetics *188*, 731.

Bellen, H.J., Levis, R.W., Liao, G., He, Y., Carlson, J.W., Tsang, G., Evans-Holm, M., Hiesinger, P.R., Schulze, K.L., Rubin, G.M., et al. (2004). The BDGP gene disruption project. Genetics *167*, 761.

Bergo, M.O., Gavino, B.J., Steenbergen, R., Sturbois, B., Parlow, A.F., Sanan, D.A., Skarnes, W.C., Vance, J.E., and Young, S.G. (2002). Defining the importance of phosphatidylserine synthase 2 in mice. J. Biol. Chem. *277*, 47701–47708.

Bhat, A.H., Dar, K.B., Anees, S., Zargar, M.A., Masood, A., Sofi, M.A., and Ganie, S.A. (2015). Oxidative stress, mitochondrial dysfunction and neurodegenerative diseases; a mechanistic insight. Biomed. Pharmacother. *74*, 101–110.

Borisenko, G.G., Matsura, T., Liu, S.X., Tyurin, V.A., Jianfei, J., Serinkan, F.B., and Kagan, V.E. (2003). Macrophage recognition of externalized phosphatidylserine and phagocytosis of apoptotic Jurkat cells–existence of a threshold. Arch. Biochem. Biophys. *413*, 41–52.

Brand, A.H., and Perrimon, N. (1993). Targeted gene expression as a means of altering cell fates and generating dominant phenotypes. Development *118*, 401–415.

Brent, J., Werner, K., and McCabe, B.D. (2009). Drosophila larval NMJ immunohistochemistry. J. Vis. Exp. 1108. https://doi.org/10.3791/1108.

Brink, D.L., Gilbert, M., Xie, X., Petley-Ragan, L., and Auld, V.J. (2012). Glial processes at the Drosophila larval neuromuscular junction match synaptic growth. PLoS One *7*, e37876.

Brown, D. (2008). Video Modeling: Combining Dynamic Model Simulations with Traditional Video Analysis.

Buccoliero, R., Bodennec, J., Van Echten-Deckert, G., Sandhoff, K., and Futerman, A.H. (2004). Phospholipid synthesis is decreased in neuronal tissue in a mouse model of Sandhoff disease. J. Neurochem. *90*, 80–88.

Choi, J.Y., Wu, W.I., and Voelker, D.R. (2005). Phosphatidylserine decarboxylases as genetic and biochemical tools for studying phospholipid traffic. Anal. Biochem. *347*, 165–175.

Chotard, C., and Salecker, I. (2007). Glial cell development and function in the Drosophila visual system. Neuron Glia Biol. *3*, 17–25.

Chung, H.L., Wangler, M.F., Marcogliese, P.C., Jo, J., Ravenscroft, T.A., Zuo, Z., Duraine, L., Sadeghzadeh, S., Li-Kroeger, D., Schmidt, R.E., et al. (2020). Loss- or gain-of-function mutations in ACOX1 cause axonal loss via different mechanisms. Neuron *106*, 589–606.e586.

Crook, T., Petrie, W., Wells, C., and Massari, D.C. (1992). Effects of phosphatidylserine in Alzheimer's disease. Psychopharmacol. Bull. *28*, 61–66.

Crook, T.H., Tinklenberg, J., Yesavage, J., Petrie, W., Nunzi, M.G., and Massari, D.C. (1991). Effects of phosphatidylserine in age-associated memory impairment. Neurology *41*, 644–649.

Duffy, J.B. (2002). GAL4 system in drosophila: a fly geneticist's swiss army knife. genesis *34*, 1–15.

Edwards, T.N., and Meinertzhagen, I.A. (2010). The functional organisation of glia in the adult brain of Drosophila and other insects. Prog. Neurobiol. *90*, 471–497.

Eskelinen, E.L., Reggiori, F., Baba, M., Kovacs, A.L., and Seglen, P.O. (2011). Seeing is believing: the impact of electron microscopy on autophagy research. Autophagy *7*, 935–956.

Etchegaray, J.I., Elguero, E.J., Tran, J.A., Sinatra, V., Feany, M.B., and McCall, K. (2016). Defective phagocytic corpse processing results in neurodegeneration and can Be rescued by TORC1 activation. J. Neurosci. *36*, 3170–3183.

Fadok, V.A., de Cathelineau, A., Daleke, D.L., Henson, P.M., and Bratton, D.L. (2001). Loss of phospholipid asymmetry and surface exposure of phosphatidylserine is required for phagocytosis of apoptotic cells by macrophages and fibroblasts. J. Biol. Chem. *276*, 1071–1077.

Fadok, V.A., Voelker, D.R., Campbell, P.A., Cohen, J.J., Bratton, D.L., and Henson, P.M. (1992). Exposure of phosphatidylserine on the surface of apoptotic lymphocytes triggers specific recognition and removal by macrophages. J. Immunol. *148*, 2207–2216.

Fergestad, T., Olson, L., Patel, K.P., Miller, R., Palladino, M.J., and Ganetzky, B. (2008). Neuropathology in Drosophila mutants with increased seizure susceptibility. Genetics *178*, 947–956.

Freeman, M.R. (2015). Drosophila central nervous system glia. Cold Spring Harb. Perspect. Biol. *7*, a020552.

Gaschler, M.M., and Stockwell, B.R. (2017). Lipid peroxidation in cell death. Biochem. Biophys. Res. Commun. *482*, 419–425.

Gong, Y., Sasidharan, N., Laheji, F., Frosch, M., Musolino, P., Tanzi, R., Kim, D.Y., Biffi, A., El Khoury, J., and Eichler, F. (2017). Microglial dysfunction as a key pathological change in adrenomyeloneuropathy. Ann. Neurol. *82*, 813–827.

Griffin, E.N., and Ackerman, S.L. (2020). Lipid metabolism and axon degeneration: an ACOX1 balancing act. Neuron *106*, 551–553.

Hakim-Mishnaevski, K., Flint-Brodsly, N., Shklyar, B., Levy-Adam, F., and Kurant, E. (2019). Glial phagocytic receptors promote neuronal loss in adult Drosophila brain. Cell Rep. *29*, 1438–1448.e1433.

Hayashi, S., Ito, K., Sado, Y., Taniguchi, M., Akimoto, A., Takeuchi, H., Aigaki, T., Matsuzaki, F., Nakagoshi, H., Tanimura, T., et al. (2002). GETDB, a database compiling expression patterns and molecular locations of a collection of gal4 enhancer traps. Genesis *34*, 58–61.

Heemels, M.-T. (2016). Neurodegenerative diseases. Nature *539*, 179.

Heiss, W.D., Kessler, J., Mielke, R., Szelies, B., and Herholz, K. (1994). Long-term effects of phosphatidylserine, pyritinol, and cognitive training in Alzheimer's disease. A neuropsychological, EEG, and PET investigation. Dementia *5*, 88–98.

Hu, Y., Flockhart, I., Vinayagam, A., Bergwitz, C., Berger, B., Perrimon, N., and Mohr, S.E. (2011). An integrative approach to ortholog prediction for disease-focused and other functional studies. BMC Bioinformatics *12*, 357.

Irvine, G.B., El-Agnaf, O.M., Shankar, G.M., and Walsh, D.M. (2008). Protein aggregation in the brain: the molecular basis for Alzheimer's and Parkinson's diseases. Mol. Med. *14*, 451–464.

Jena, N.R. (2012). DNA damage by reactive species: mechanisms, mutation and repair. J. Biosci. *37*, 503–517.

Kim, H.Y., Huang, B.X., and Spector, A.A. (2014). Phosphatidylserine in the brain: metabolism and function. Prog. lipid Res. *56*, 1–18.

Kondo, S., and Ueda, R. (2013). Highly improved gene targeting by germline-specific Cas9 expression in Drosophila. Genetics *195*, 715–721.

Kretzschmar, D., Hasan, G., Sharma, S., Heisenberg, M., and Benzer, S. (1997). The swiss cheese mutant causes glial hyperwrapping and brain degeneration in Drosophila. J. Neurosci. *17*, 7425–7432.

Kuebler, D., and Tanouye, M.A. (2000). Modifications of seizure susceptibility inDrosophila. J. Neurophysiol. *83*, 998–1009.

Lee, Y.M., and Sun, Y.H. (2015). Drosophila as a model to study the role of glia in neurodegeneration. J. Neurogenet. *29*, 69–79.

Leventis, P.A., and Grinstein, S. (2010). The distribution and function of phosphatidylserine in cellular membranes. Annu. Rev. Biophys. *39*, 407–427.

Li, Z., Zhang, J., and Sun, H. (2015). Increased plasma levels of phospholipid in Parkinson's disease with mild cognitive impairment. J. Clin. Neurosci. *22*, 1268–1271.

Liu, L., Zhang, K., Sandoval, H., Yamamoto, S., Jaiswal, M., Sanz, E., Li, Z., Hui, J., Graham, B.H., Quintana, A., et al. (2015). Glial lipid droplets and ROS induced by mitochondrial defects promote neurodegeneration. Cell *160*, 177–190.

Midorikawa, R., Yamamoto-Hino, M., Awano, W., Hinohara, Y., Suzuki, E., Ueda, R., and Goto, S. (2010). Autophagy-dependent rhodopsin degradation prevents retinal degeneration in Drosophila. J. Neurosci. *30*, 10703–10719.

Miller, D.L., Ballard, S.L., and Ganetzky, B. (2012). Analysis of synaptic growth and function in Drosophila with an extended larval stage. J. Neurosci. *32*, 13776–13786.

Mizushima, N. (2007). Autophagy: process and function. Genes Development *21*, 2861–2873.

Muñoz, L.E., Lauber, K., Schiller, M., Manfredi, A.A., and Herrmann, M. (2010). The role of defective clearance of apoptotic cells in systemic autoimmunity. Nat. Rev. Rheumatol. *6*, 280.

Napoli, I., and Neumann, H. (2009). Microglial clearance function in health and disease. Neuroscience *158*, 1030–1038.

Owusu-Ansah, E., Yavari, A., and Banerjee, U. (2008). A Protocol for in Vivo Detection of Reactive Oxygen Species (Protocol Exchange).

Palladino, M.J., Hadley, T.J., and Ganetzky, B. (2002). Temperature-sensitive paralytic mutants are enriched for those causing neurodegeneration in Drosophila. Genetics *161*, 1197–1208.

Parker, L., Howlett, I.C., Rusan, Z.M., and Tanouye, M.A. (2011). Seizure and epilepsy: studies of seizure disorders in Drosophila. In International Review of Neurobiology, N. Atkinson, ed. (Academic Press), pp. 1–21.

Pavlidis, P., Ramaswami, M., and Tanouye, M.A. (1994). The Drosophila easily shocked gene: a mutation in a phospholipid synthetic pathway causes seizure, neuronal failure, and paralysis. Cell *79*, 23–33.

Pettegrew, J.W., Panchalingam, K., Hamilton, R.L., and McClure, R.J. (2001). Brain membrane phospholipid alterations in Alzheimer's disease. Neurochem. Res. *26*, 771–782.

Poon, I.K.H., Lucas, C.D., Rossi, A.G., and Ravichandran, K.S. (2014). Apoptotic cell clearance: basic biology and therapeutic potential. Nat. Rev. Immunol. *14*, 166–180.

Ravichandran, Kodi S. (2011). Beginnings of a good apoptotic meal: the find-me and eat-me signaling pathways. Immunity *35*, 445–455.

Ross, C.A., and Poirier, M.A. (2004). Protein aggregation and neurodegenerative disease. Nat. Med. *10*, S10–S17.

Salter, M.W., and Stevens, B. (2017). Microglia emerge as central players in brain disease. Nat. Med. *23*, 1018–1027.

Sarkissian, T., Timmons, A., Arya, R., Abdelwahid, E., and White, K. (2014). Detecting apoptosis in Drosophila tissues and cells. Methods *68*, 89–96.

Schenkel, L.C., and Bakovic, M. (2014). Formation and regulation of mitochondrial membranes. Int. J. Cell Biol. *2014*, 709828.

Segawa, K., and Nagata, S. (2015). An apoptotic 'Eat Me' signal: phosphatidylserine exposure. Trends Cell Biol. *25*, 639–650.

Serpell, L.C., and Smith, J.M. (2000). Direct visualisation of the beta-sheet structure of synthetic Alzheimer's amyloid. J. Mol. Biol. *299*, 225–231.

Sharon, R., Bar-Joseph, I., Frosch, M.P., Walsh, D.M., Hamilton, J.A., and Selkoe, D.J. (2003). The formation of highly soluble oligomers of alpha-synuclein is regulated by fatty acids and enhanced in Parkinson's disease. Neuron *37*, 583–595.

Sies, H. (2017). Hydrogen peroxide as a central redox signaling molecule in physiological oxidative stress: oxidative eustress. Redox Biol. *11*, 613–619.

Silva, M.T. (2010). Secondary necrosis: the natural outcome of the complete apoptotic program. FEBS Lett. *584*, 4491–4499.

Simossis, V.A., and Heringa, J. (2005). PRALINE: a multiple sequence alignment toolbox that integrates homology-extended and secondary structure information. Nucleic Acids Res. *33*, W289–W294.

Smith, R., and Taylor, J.P. (2011). Dissection and imaging of active zones in the Drosophila neuromuscular junction. J. Vis. Exp. 2676. https://doi.org/10.3791/2676.

Sousa, S.B., Jenkins, D., Chanudet, E., Tasseva, G., Ishida, M., Anderson, G., Docker, J., Ryten, M., Sa, J., Saraiva, J.M., et al. (2014). Gain-of-function mutations in the phosphatidylserine synthase 1 (PTDSS1) gene cause Lenz-Majewski syndrome. Nat. Genet. *46*, 70–76.

Starkov, A.A. (2008). The role of mitochondria in reactive oxygen species metabolism and signaling. Ann. N. Y. Acad. Sci. *1147*, 37–52.

Steenbergen, R., Nanowski, T.S., Beigneux, A., Kulinski, A., Young, S.G., and Vance, J.E. (2005). Disruption of the phosphatidylserine decarboxylase gene in mice causes embryonic lethality and mitochondrial defects. J. Biol. Chem. *280*, 40032–40040.

Stone, S.J., and Vance, J.E. (2000). Phosphatidylserine synthase-1 and -2 are localized to mitochondria-associated membranes. J. Biol. Chem. *275*, 34534–34540.

Tamura, Y., Onguka, O., Itoh, K., Endo, T., Iijima, M., Claypool, S.M., and Sesaki, H. (2012). Phosphatidylethanolamine biosynthesis in mitochondria: phosphatidylserine (PS) trafficking is independent of a PS decarboxylase and intermembrane space proteins UPS1P and UPS2P. J. Biol. Chem. *287*, 43961–43971.

Tasseva, G., Bai, H.D., Davidescu, M., Haromy, A., Michelakis, E., and Vance, J.E. (2013). Phosphatidylethanolamine deficiency in Mammalian mitochondria impairs oxidative phosphorylation and alters mitochondrial morphology. J. Biol. Chem. *288*, 4158–4173.

Thomas, R.L., and Gustafsson, A.B. (2013). Mitochondrial autophagy–an essential quality control mechanism for myocardial homeostasis. Circ. J. *77*, 2449–2454.

Thome, M.P., Filippi-Chiela, E.C., Villodre, E.S., Migliavaca, C.B., Onzi, G.R., Felipe, K.B., and Lenz, G. (2016). Ratiometric analysis of Acridine Orange staining in the study of acidic organelles and autophagy. J. Cell Sci. *129*, 4622–4632.

Ullian, E.M., Christopherson, K.S., and Barres, B.A. (2004). Role for glia in synaptogenesis. Glia *47*, 209–216.

Valadas, J.S., Esposito, G., Vandekerkhove, D., Miskiewicz, K., Deaulmerie, L., Raitano, S., Seibler, P., Klein, C., and Verstreken, P. (2018). ER

lipid defects in neuropeptidergic neurons impair sleep patterns in Parkinson's disease. Neuron *98*, 1155–1169.e1156.

Vance, J.E. (2014). MAM (mitochondria-associated membranes) in mammalian cells: lipids and beyond. Biochim. Biophys. Acta *1841*, 595–609.

Vance, J.E., and Steenbergen, R. (2005). Metabolism and functions of phosphatidylserine. Prog. lipid Res. *44*, 207–234.

Vance, J.E., and Tasseva, G. (2013). Formation and function of phosphatidylserine and phosphatidylethanolamine in mammalian cells. Biochim. Biophys. Acta *1831*, 543–554.

Von Bernhardi, R., Eugenin-von Bernhardi, L., and Eugenin, J. (2015). Microglial cell dysregulation in brain aging and neurodegeneration. Front. Aging Neurosci. *7*, 124.

Wang, S., Zhang, S., Liou, L.C., Ren, Q., Zhang, Z., Caldwell, G.A., Caldwell, K.A., and Witt, S.N. (2014). Phosphatidylethanolamine deficiency disrupts alpha-synuclein homeostasis in yeast and worm models of Parkinson disease. Proc. Natl. Acad. Sci. U S A *111*, E3976–E3985.

White, C.J., and Gallin, J.I. (1986). Phagocyte defects. Clin. Immunol. *40*, 50–61.

Williams, D., Vicogne, J., Zaitseva, I., McLaughlin, S., and Pessin, J.E. (2009). Evidence that electrostatic interactions between vesicle-associated membrane protein 2 and acidic phospholipids may modulate the fusion of transport vesicles with the plasma membrane. Mol. Biol. Cell *20*, 4910–4919.

Yang, X., Liang, J., Ding, L., Li, X., Lam, S.-M., Shui, G., Ding, M., and Huang, X. (2019). Phosphatidylserine synthase regulates cellular homeostasis through distinct metabolic mechanisms. PLoS Genet. *15*, e1008548.

STAR★METHODS

KEY RESOURCES TABLE

REAGENT or RESOURCE	SOURCE	IDENTIFIER
Antibodies		
Mouse anti-GFP	DSHB	Cat# GFP-G1, RRID: AB_2619561
Rabbit anti-GFP	Abcam	Cat# ab183734, RRID:AB_2732027
Mouse anti-Repo	DSHB	Cat# 8D12 anti-Repo, RRID:AB_528448
Mouse anti-Elav	DSHB	Cat# ELAV 9F8A9, RRID:AB_2314364
Mouse anti-CSP	DSHB	Cat# DCSP-1 (ab49), RRID:AB_2307345
Rabbit anti-cleaved caspase 3	Cell signal	Cat# 9661, RRID:AB_2341188
Goat anti-Mouse Alexa 488	Invitrogen	Cat# A-11001, RRID:AB_2534069
Goat anti-Mouse Alexa 594	Invitrogen	Cat# A-11005, RRID:AB_2534073
Goat anti-Rabbit Alexa 488	Invitrogen	Cat# A21222, RRID:AB_10373853
Goat anti-Rabbit Alexa 594	Invitrogen	Cat# A-11072, RRID:AB_2534116
Alexa 594 AffiniPure Goat Anti-HRP	Jackson ImmunoResearch Labs	Cat# 123-585-021, RRID: AB_2338966
Bacterial and virus strains		
DH5α Chemically Competent E. coli	enzynomics	Cat# CP010
Chemicals, peptides, and recombinant proteins		
4% paraformaldehyde	Biosesang	Cat# PC2031-050-00
20X PBS	Biosesang	Cat# PR2007-100-00
Triton X-100	Sigma-Aldrich	Cat# X100
Fluoromount-G	SouthernBiotech	Cat# 0100-01
Schneider's Drosophila Medium (SDM)	Gibco	Cat# 21720024
Dihydroethidium (DHE)	Invitrogen	Cat# D11347
C11-BODIPY 581/591	Invitrogen	Cat# D3861
Acridine Orange (AO)	Invitrogen	Cat# A1301
RealTime-Glo™ Annexin V Apoptosis and Necrosis Assay	Promega	Cat# JA1011
Ethyl alcohol, anhydrous, 99.9%	Samchun	Cat# E0243
Chloroform, 99.5%	Samchun	Cat# C0584
Acetic acid (glacial) 100%	Merck	Cat# 100063
Paraplast	Leica	Cat# 39601006
Paraplast plus	Sigma-Aldrich	Cat# P3683
Hematoxylin	Sigma-Aldrich	Cat# 105175
Eosin Y	Sigma-Aldrich	Cat# 318906
Xylene, 99.9%	Samchun	Cat# X0097
5X All-In-One RT MasterMix (with AccuRT Genomic DNA Removal Kit)	Abm	Cat# G492
TOPreal qPCR 2X PreMix (SYBR green with low ROX)	Enzynomics	Cat# RT500S
iTaq Universal SYBR Green Supermix	Bio-Rad	Cat# 1725120
4% glutaraldehyde	Ted Pella	Cat# 18427
0.1 M cacodylate buffer	Ted Pella	Cat# 18851
100% propylene	EMS	Cat# 20401
eponate 812 resin	Ted Pella	Cat# 18005
Uranyl acetate	Ted Pella	Cat# 19481
Lead citrate	EMS	Cat# 17800

(*Continued on next page*)

Continued

REAGENT or RESOURCE	SOURCE	IDENTIFIER
Critical commercial assays		
RNeasy Plus Mini Kit	Qiagen	Cat# 74134
Deposited data		
FlyBase	-	http://flybase.org
Experimental models: Organisms/strains		
Pss^{15}	BDSC	RRID: BDSC_2215
Pss^{32}	BDSC	RRID: BDSC_11632
Pss^{GAL4}	Kyoto Stock Center	RRID: Kyoto Stock Center_104172
Pss$^{\Delta 1}$	Jeon lab (This paper)	N/A
Df(3L)BSC448	BDSC	RRID: BDSC_24952
da-GAL4	BDSC	RRID: BDSC_55851
Act-GAL4	BDSC	RRID: BDSC_4414
repo-GAL4	BDSC	RRID: BDSC_7415
elav-GAL4	BDSC	RRID: BDSC_8765
D42-GAL4	BDSC	RRID: BDSC_8816
alrm-GAL4	BDSC	RRID: BDSC_67031
Mz97-GAL4	BDSC	RRID: BDSC_9488
UAS-mCherry.nls	BDSC	RRID: BDSC_38424
UAS-GFP.nls	BDSC	RRID: BDSC_4776
UAS-mCD8.GFP	BDSC	RRID: BDSC_32186
NP2222-GAL4	Kyoto Stock Center	RRID: Kyoto Stock Center_112830
NP6293-GAL4	Kyoto Stock Center	RRID: Kyoto Stock Center_105188
NP2276-GAL4	Kyoto Stock Center	RRID: Kyoto Stock Center_112853
UAS-Pss RNAi	VDRC	RRID: VDRC_V5391
y^{1} *v*^{1} *nos-phiC31; attP40*	NIG-fly	RRID: SHIGEN TBX-0002
y^{2} *cho*^{2} *v*^{1}	NIG-fly	RRID: SHIGEN TBX-0004
y^{2} *cho*^{2} *v*^{1}*; Sp/CyO*	NIG-fly	RRID: SHIGEN TBX-0009
y^{2} *cho*^{2} *v*^{1}*; attP40{nos-Cas9}/CyO*	NIG-fly	RRID: SHIGEN CAS-0001
y^{2} *cho* ^{2} *v*^{1}*; Pr Dr/TM6C, Sb Tb*	NIG-fly	RRID: SHIGEN TBX-0010
UAS-Pss	Jeon lab (This paper)	N/A
Oligonucleotides		
Pss$^{\Delta 1}$ gRNA top oligo: CTTCGAACGTGGATGAGAA TCTCT	Bioneer	N/A
Pss$^{\Delta 1}$ gRNA bottom oligo: AAACAGAGATTCTCAT CCACGTTC	Bioneer	N/A
qRT-PCR primer for *Rp49* forward oligo: FW 5′-ACA GGCCCAAGATCGTGAAGA-3′	Bioneer	N/A
qRT-PCR primer for *Rp49* reverse oligo: RV 5′-CGCA CTCTGTTGTCGATACCCT-3′	Bioneer	N/A
qRT-PCR primer for *Pss* forward oligo: FW 5′-ACAGG CCCAAGATCGTGAAGA-3′	Bioneer	N/A
qRT-PCR primer for *Pss* reverse oligo: RV 5′-CGCACTC TGTTGTCGATACCCT-3′	Bioneer	N/A

(*Continued on next page*)

Continued

REAGENT or RESOURCE	SOURCE	IDENTIFIER
Software and algorithms		
BLAST	NCBI	https://blast.ncbi.nlm.nih.gov/Blast.cgi
PRALINE	(Simossis and Heringa, 2005) https://doi.org/10.1093/nar/gki390	https://www.ibi.vu.nl/programs/pralinewww/
Rotor-Gene Q Software	Qiagen	https://www.qiagen.com/kr/resources/resourcedetail?id=8435805b-2c5d-4fa9-948c-a43de75a7ee1&lang=en
CFX Manger Software	Bio-Rad	https://www.bio-rad.com/en-kr/sku/1845000-cfx-manager-software?ID=1845000
QuantStudio 5 Real-Time PCR System Software	ThermoFisher	https://www.thermofisher.com/kr/en/home/global/forms/life-science/quantstudio-3-5-software.html
ImageJ	Version 2.1.0	https://imagej.nih.gov/ij/
Zen Black	Zeiss	https://www.zeiss.com/microscopy/us/products/microscope-software/zen-lite.html
LAS X	Leica	https://www.leica-microsystems.com/products/microscope-software/p/leica-las-x-ls/
MetaMorph	Version 7.8.6.0	https://www.moleculardevices.com/products/cellular-imaging-systems/acquisition-and-analysis-software/metamorph-microscopy#gref
Tracker	Version 5.1.5	https://tracker.physlets.org/

RESOURCE AVAILABILITY

Lead contact and materials availability

Further information and requests for resources and reagents should be directed to and will be fulfilled by the Lead Contact, Sang-Hak Jeon (jeonsh@snu.ac.kr). All fly lines and plasmids generated in this study are available from the Lead Contact without restriction.

Data and code availability

All data reported in this paper will be shared by the lead contact upon request. This paper does not report original code. Any additional information required to reanalyze the data reported in this paper is available from the lead contact upon request.

EXPERIMENTAL MODEL AND SUBJECT DETAILS

Drosophila melanogaster strains

Pss mutant alleles used for this experiment were designated according to the last two digits taken from the stock number: Pss^{15} (BL22115, w^{1118}; *P{EPg}*$Pss^{HP31723}$), Pss^{32} (BL11632, *P{PZ}*Pss^{04521} ry^{506} /*TM3,* ry^{RK} Sb^{1} Ser^{1}), and Pss^{GAL4} (#104172, *w*; P{GawB}*Pss^{NP2363} / *TM3,* Sb^{1} Ser^{1}) (Bellen et al., 2004, 2011; Hayashi et al., 2002). We used the Pss^{32} line to collect virgins for crosses to generate *trans*-heterozygous mutants ($Pss^{32/15}$, $Pss^{32/GAL4}$, $Pss^{32/\Delta 1}$, Pss^{32}/*Df*), and used *Canton-S* as female parent to generate heterozygous mutants ($Pss^{32/+}$, $Pss^{\Delta 1/+}$) to make their backgrounds same in w^{+}. *Canton-S* was used as a control. For the transgenic manipulations, the GAL4-UAS system was employed (Brand and Perrimon, 1993). We obtained Pss^{15} (BL22115), Pss^{32} (BL11632), Pss^{GAL4} (BL104172), *Df(3L)BSC448* (BL24952), *da-GAL4* (BL55851), *Act-GAL4* (BL4414), *repo-GAL4* (BL7415), *elav-GAL4* (BL8765), *D42-GAL4* (BL8816), *alrm-GAL4* (BL67031), *Mz97-GAL4* (BL9488), *UAS-mCherry.nls* (BL38424), *UAS-GFP.nls* (BL4776) and *UAS-mCD8.GFP* (BL32186) from the Bloomington *Drosophila* Stock Center (BDSC); Pss^{GAL4}, *NP2222-GAL4* (#112830), *NP6293-GAL4* (#105188), and *NP2276-GAL4* (#112853) from the Kyoto Stock Center; and *UAS-Pss RNAi* (V5391) from the Vienna *Drosophila* Resource Center (VDRC). The V5391 was already validated in a recent study (Yang et al., 2019) as it dramatically reduced the expression level of *Pss* in salivary gland (*ppl>Pss RNAi*, almost 90% reduced). Flies were raised in vials containing cornmeal–yeast–agar medium at 22°C or 25°C during development and at 29°C after eclosion, with 50% relative humidity and a 12 h:12 h light:dark cycle. Except for the complementary test, we used only male progenies for all the other assays on adult flies.

METHOD DETAILS

Generation of *Pss*$^{\Delta 1}$ and *UAS-Pss*

We employed the CRISPR/Cas9 system to generate a small deletion in the 2nd exon of the *Pss* gene, as described previously (Kondo and Ueda, 2013). To construct gRNA, two complementary oligonucleotides targeting a region in the 2nd exon, 'CTTCGAACGTGGATGAGAATCTCT' and 'AAACAGAGATTCTCATC CACGTTC', were annealed and cloned into the pBFv-U6.2 vector (NIG-fly) at the *Bbs*I site, and the resulting recombinant plasmids were injected into y^1 v^1 *nos-phiC31; attP40* host embryos. Subsequent methods for producing a gRNA-mediated deletion line followed the previously described procedures (Kondo and Ueda, 2013). G0 males that survived to adulthood were individually mated with y^2 cho^2 v^1 (NIG-fly). Male offspring showing wild-type eye color (i.e., transformants) were crossed with y^2 cho^2 v^1; *Sp/CyO* (NIG-fly) virgins, and then the transgenic line was balanced and established as a stock (*U6-Pss-gRNA*). Male flies of this line were crossed with y^2 cho^2 v^1; *attP40{nos-Cas9}/CyO* (NIG-Fly), which express the Cas9 protein specifically in the germ line. The male founders containing both *U6-Pss-gRNA* and *nos-Cas9* transgenes were mated with y^2 cho^2 v^1; *Pr Dr/TM6C, Sb Tb* flies. Offspring balanced with *TM6C, Sb Tb* were collected to establish a stock and used for molecular characterization. To generate *UAS-Pss* transgenic lines, a full-length cDNA was cloned into a pUAST vector, and the resulting plasmid was used for conventional germ-line transformation.

Protein homology and alignment of *Pss*

Pss gene sequence and protein sequence information were obtained from the FlyBase (http://flybase.org). Protein BLAST was conducted using web-based software (https://blast.ncbi.nlm.nih.gov/Blast.cgi) to determine the similarities between fly PSS and human PSSs. Amino acid sequence alignment was performed with PRALINE (Simossis and Heringa, 2005).

Quantitative real-time PCR

Total RNA was extracted from pupae using RNeasy Plus Mini Kit (Qiagen, #74134), and then ~1.0 μg RNA was reverse transcribed to synthesize cDNA using a 5X All-In-One RT MasterMix with AccuRT Genomic DNA Removal Kit (Abm, G492). qPCR was performed with TOPreal qPCR 2X PreMix (SYBR green with low ROX, enzynomics) and Rotor-Gene Q (QIAGEN) or with iTaq Universal SYBR Green Supermix (BIO-RAD) and CFX96 Touch Real-Time PCR Detection System (BIO-RAD) or QuantStudio™ 5 System (Thermo Fisher Scientific). Rp49 was used for normalization. The following primers were used for qPCR:

Rp49-for (5′-ACAGGCCCAAGATCGTGAAGA-3′)

Rp49-rev (5′-CGCACTCTGTTGTCGATACCCT-3′)

Pss-for (5′-ATGAAGAAGCGCACTAATTCACG-3′)

Pss-rev (5′-CCTGATTTGTAGGCGGGATG-3′)

Longevity, climbing ability, and bang sensitivity

For all assays, newly eclosed flies were collected and kept at 29°C until used. For the longevity assay, each genotype was collected at eclosion, divided into vials (up to 20 flies per vial), and then incubated at 29°C. Flies were transferred to fresh vials every 3 days, and the number of dead flies was counted. Survival rates were calculated from the total population. To test climbing ability, we made a climbing kit with 5 vials (diameter: 2.6cm, height: 27.7cm) and a frame that enables us to compare up to 5 alleles at once. 3, 10, 20, or 30-day-old flies were transferred to an empty vial (each containing up to 20 flies). The vials in the frame were gently tapped to force all flies to the bottom and then videotaped for 10 s. This was repeated ten times for each vial, and this was considered as one set. 3-5 sets were analyzed by Tracker software (Brown, 2008) (https://tracker.physlets.org/) for final data. Error bars for the climbing assay are SEM. For the bang sensitivity test, 3-day-old flies were transferred to an empty vial and vortexed for 5 s at maximum speed (3000 rpm). For each individual fly, we measured the time from the end of the impact to the moment that flies right themselves. At least 14 flies were tested for each genotype.

Detection of vacuoles in the brain

To detect vacuoles in the brain, fly heads were fixed in fresh Carnoy's solution (ethanol:chloroform:acetic acid at 6:3:1) at 4°C for at least 24 h, washed, serially dehydrated with ethanol, and paraffin-embedded using standard histological procedures (Palladino et al., 2002). Serial 5 μm sections were stained with hematoxylin and eosin and examined under a light microscope. Images were taken with a DE/Axio Imager A1 microscope (Carl Zeiss) equipped with a DE/Axiocam HR. The diameter of the vacuoles was measured by ImageJ. The total numbers of vacuoles with diameter from 3μm to 6μm and over 6μm in each fly brain were divided by the total number of slices of each fly brain to obtain the average number of vacuoles per slice. For each genotype, at least 11 heads were used.

NMJ analyses and larval roll-over assay

NMJs were dissected from wandering third instar larvae, as described previously (Smith and Taylor, 2011). The NMJs between the 6/7 muscles of the A3 segment were stained with anti-HRP and anti-CSP. An Intravital multi-photon confocal laser scanning microscope (IMP-LSM; LSM 780 NLO, Carl Zeiss) was used for observing and photographing NMJs. ImageJ was used for the quantification of boutons, branches, and NMJ length. Synaptic branches with two or more synaptic boutons were considered branches, according to (Miller et al., 2012).

For the larval roll-over assay, a third instar larva was placed on an apple juice plate. After a brief adjustment period, the larva was gently inverted (ventral side up). The time taken for the original posture (dorsal side up) to be restored was measured. For each genotype, at least 20 larvae were tested.

Immunohistochemistry

Mouse anti-GFP (G1-S, 1:25, Developmental Studies Hybridoma Bank (DSHB)), rabbit anti-GFP (1:25, Abcam), mouse anti-Repo (8D12, 1:20, DSHB), mouse anti-Elav (9F8A9, 1:40, DSHB), and mouse anti-CSP (ab49, 1/20, DSHB) were used as primary antibodies. For secondary antibodies, we used goat anti-mouse-IgG and anti-rabbit-IgG conjugated with Alexa Fluor 488 or Alexa Fluor 594 (1:1000 dilution, Invitrogen) and Alexa Fluor 594-conjugated AffiniPure Goat Anti-Horseradish Peroxidase (1:400, Jackson ImmunoResearch).

Tissue was fixed with 4% paraformaldehyde for 30 min, washed in PT (1X PBS, 0.1% Triton X-100), incubated with primary antibodies overnight at 4°C, and then washed again before incubation with secondary antibodies for 1–2 h at room temperature. Tissue was thoroughly rinsed in PT and mounted with Fluoromount-G for imaging.

Detection of ROS in brain tissue

Fly brains were dissected in Schneider's medium (SDM). After brief washing with SDM, the brains were incubated for 5 min either with 150 μL DHE (final concentration 30 μM) to detect ROS or with C11-BODIPY(581/591) (final concentration 2 μM) to measure lipid peroxidation. After washing three times in SDM, brains were mounted with Fluoromount-G and then observed immediately with an Intravital multi-photon confocal laser scanning microscope (IMP-LSM; LSM 780 NLO, Carl Zeiss). Images were obtained as Z series with the same interval for the whole brain. Z series images were merged by ImageJ (Image-Stacks-Z projection-SUM slices), and then the fluorescence intensity was measured. To compare the fluorescence intensity, a ratio was calculated by dividing the fluorescence value from the mutant brain by the fluorescence value from the wild-type brain obtained immediately after the mutant.

Detection of cell death in brain tissue

Acridine orange (AO) staining and anti-caspase 3 immunohistochemistry were used to detect dying cells in adult brains. The chemicals were prepared as follows: 1.3 μL of 1 mM AO (Invitrogen, A1301) in 1 mL of 1X PBS; rabbit anti-cleaved caspase 3 antibody (#9661, 1:100, Cell signal); and Alexa Fluor 594 conjugated goat anti-rabbit-IgG (1:1000, Invitrogen).

For AO staining, fly brains were dissected in PBS, washed with PBS, and then incubated in 150 μL AO for 10 min. The tissue was washed three times with PBS, mounted in Fluoromount-G, and observed immediately with an Intravital multi-photon confocal laser scanning microscope (IMP-LSM; LSM 780 NLO, Carl Zeiss). Each observation was conducted under the following conditions: single-strand DNA and RNA

(excitation: 488 nm, emission: 650 nm); lysosome (excitation: 561 nm, emission: 579–620 nm). Images were analyzed in the same way as described above in ROS detection.

Transmission electron microscopy

Fly heads without the proboscis were fixed with 2% glutaraldehyde and 2% paraformaldehyde in phosphate buffer (pH 7.4) for 1h at 4°C and then postfixed osmium tetroxide for 40 min at 4°C. The samples were dehydrated in a graded series of ethanol. The samples were treated with graded propylene oxide series and embedded into Epon. The sections were then ultra-thin sectioned in 80-nm and placed on copper grid. The final samples were stained with uranyl acetate and lead citrate. After the observed using a transmission electron microscope (JEOL-2100F, USA, 200kV) at the Korea Basic Science Institute, Chuncheon Center.

Detection of necrosis

We used the necrosis detection reagent (1000X) from the RealTime-Glo™ Annexin V Apoptosis and Necrosis Assay (Promega, JA1011). Reagents were diluted to 1X in SDM immediately before use. Fly heads without the proboscis were stained in 1X necrosis detection reagent for 2 h at room temperature. Then, the tissue was washed three times with SDM. The cuticles were removed gently and quickly, and the brains were mounted in Fluoromount-G. Images were obtained with an Olympus BX51 microscope, a Q Imaging optiMOS camera, and MetaMorph software.

QUANTIFICATION AND STATISTICAL ANALYSIS

Quantified data were analyzed statistically with the Excel program's data analysis tools for the f-test and the t-test. Log-rank test was used to compare survival (lifespan) curves. Statistical significance is shown as follows: *$p < 0.05$, **$p < 0.01$, ***$p < 0.001$. $p > 0.05$ was considered not significant (n.s.).